

**CFD ANALYSIS OF AHMED BODY WITH
DIFFERENT YAW ANGLES**

**A THESIS SUBMITTED TO THE GRADUATE
SCHOOL OF APPLIED SCIENCES
OF
NEAR EAST UNIVERSITY**

**By
MUHAMMAD MAHAD KALEEM**

**In Partial Fulfilment of the Requirements for
the Degree of Master of Science
in
Mechanical Engineering**

NICOSIA, 2019

**CFD ANALYSIS OF AHMED BODY WITH
DIFFERENT YAW ANGLES**

**A THESIS SUBMITTED TO THE GRADUATE
SCHOOL OF APPLIED SCIENCES
OF
NEAR EAST UNIVERSITY**

**By
MUHAMMAD MAHAD KALEEM**

**In Partial Fulfilment of the Requirements for
the Degree of Master of Science
in
Mechanical Engineering**

NICOSIA, 2019

**Muhammad MahadKaleem: CFD ANAYSIS OF AHMED BODY WITH
DIFFERENT YAW ANGLES**

**Approval of Director of Graduate School of
Applied Sciences**

Prof. Dr. Nadire CAVUS

**We certify that thesis is satisfactory for the award of the degree of Masters of Science
in Mechanical Engineering**

Examining Committee in Charge:

Assist. Prof. Dr. Elbrus Bashir IMANOV

Committee Chairman, Department of
Computer Engineering, NEU

Assist. Prof. Dr. Ali EVCIL

Department of Mechanical
Engineering, NEU

Prof. Dr. Nuri KAYANSAYAN

Supervisor, Department of
Mechanical Engineering, NEU

I hereby declare that all information in this document has been obtained and presented in accordance with academic rules and ethical conduct. I also declare that, as required by these rules and conduct, I have fully cited and referenced all material and results that are not original to this work.

Name, Last name:

Signature:

Date

ACKNOWLEDGEMENTS

First of all, I would like to express my deep gratitude to the Almighty ALLAH who created this transitory world. Also to Prophet Mohammad (PBUH) to provide knowledge and guidance and always been an inspiration for me to complete me my thesis.

I am very grateful to my supervisor Prof. Dr. Nuri KAYANSAYAN for his sincere guidance, untiring cooperation, valuable advice and endless inspiration that helps me to overcome the entire problem during the course of study and preparation of thesis.

There is a long list of people that I would like to thank especially to my parents and my wife who has been my strongest motivation for the completion of thesis. I would also like to thank my best college Muhammad Abid Khan who has provided a valuable help throughout the study.

**Dedicated to my parents, wife, brothers
and Siblings ...**

ABSTRACT

Ahmed body considered to be the benchmark for the automotive industry that is used to determine the drag around the region of the body. There are lots of experimental results that are obtained through different methods including Sub-grid Scale. However, this article belongs to findings of drag coefficient with different yaw angles which are used previously. Firstly, we determine values of friction that are related to the car's speed. Then analyze the value of drag coefficient against yaw angles ranging from 0° to 80° . We also determine the velocity and the pressure profiles in terms of orientation of the car and identify the outcome up to the angle of 60° . It is concluded that the data obtained by CFD analysis around the car is comparable with experimental results.

Keywords: Ahmed body; yaw angles; Reynolds number; CFD analysis; sub-grid scale

ÖZET

Ahmed gövdesi, vücut bölgesindeki sürtünmeyi belirlemek için kullanılan otomotiv endüstrisi için bir kriter olarak kabul edildi. Alt Izgara Ölçe i dahil olmak üzere farklı yöntemlerle elde edilen birçok deneysel sonuç vardır. Bununla birlikte, bu makale daha önce kullanılan farklı yalpa açıları ile sürtünme katsayısı bulgularına aittir. İlk olarak, otomobilin hızıyla ilgili olan sürtünme değerlerini belirleriz. Sonra sürüklenme katsayısının değerini 0° ile 80° arasında değişen yalpalama açılarına karşı analiz edin. Ayrıca kabinin oryantasyonu açısından hız ve basınç profillerini belirler ve sonucu 60° 'ye kadar olan açıyla belirleriz. Araç çevresinde CFD analizi ile elde edilen verilerin deneysel sonuçlarla karşılaştırılabilir olduğunu sonucuna varılmıştır.

Anahtar kelimeler: Ahmed gövdesi; yalpa açıları; Reynolds sayısı; CFD analizi; alt ızgara ölçe i

TABLE OF CONTENTS

ACKNOWLEDGEMENTS	ii
ABSTRACT	iv
ÖZET	v
LIST OF TABLES	ix
LIST OF FIGURES	x
LIST OF SYMBOLS	xiii
LIST OF ABBREVIATIONS	xiv

CHAPTER 1: INTRODUCTION

1.1 Automotive Industry	1
1.2 Ahmed Body	1
1.3 Research Aim	2
1.4 Thesis Outline	2

CHAPTER 2: LITERATURE REVIEW AND THESIS

2.1 Literature Review	4
2.2 CFD Analysis	5
2.3 Components of CFD.....	6
2.3.1 Pre-Processor.....	6
2.3.2 Solver	7
2.3.3 Post-Processor	7
2.4 Advantages of CFD Analysis	8
2.5 Disadvantages of CFD Analysis	8
2.6 Drag Coefficient.....	8
2.7 Boundary Conditions.....	9
2.8 Continuity Equation	9

2.8.1 Conservation of Mass	9
2.9 Navier Stokes Equation	10
2.10 Skin Friction Coefficient	11
2.11 Wall Shear Stress	12
2.12 Friction Velocity	12
2.13 Wall Distance	13

CHAPTER 3: METHODOLOGY

3.1 Geometry	15
3.2 Meshing	23
3.2.1 Nodes	24
3.2.2 Division of Grids:	24
3.2.3 Calculations for determining Boundary Layer Thickness	26
3.2.4 Grid Size	34
3.2.5 Number of Grid size	34
3.3 Setup	36
3.3.1 Scheme	44
3.3.2 Spatial Discretization	44

CHAPTER 4: RESULTS AND DISCUSSIONS

4.1 Pressure and Velocity Profiles	50
4.1.1 20° Angle	50
4.1.2 0° Angle	52
4.1.3 40° Angle	53
4.1.4 60° Angle	54
4.1.5 80° Angle	55
4.2 Drag Coefficient	56
4.3 Reynolds Number and Drag Coefficient	58

CHAPTER 5: CONCLUSIONS AND RECOMMENDATIONS

5.1 Conclusions 61
5.2 Recommendations 62

REFERENCES 63

LIST OF TABLES

Table 3.1: Description of divisions for Meshing	32
Table 4.1: Drag Coefficient for different Yaw Angles.....	56
Table 4.2: Value of Drag coefficient of experimental results and the present findings against Reynolds number	59

LIST OF FIGURES

Figure 1.1: Ahmed body model representation in 2D	2
Figure 2.1: Conservation of mass in and out of a body	9
Figure 3.1: Ansys workbench for analysis of problem.....	15
Figure 3.2: Design-Modeler Geometry domain	16
Figure 3.3: Selection of XY Plane.....	17
Figure 3.4: Ahmed body dimensions in millimeters	17
Figure 3.5: Dimension of horizontal and vertical dimensions of body in meter	18
Figure 3.6: Defining yaw angle	19
Figure 3.7: Use of commands of Fillet and Trim	19
Figure 3.8: All dimensions used in body.....	20
Figure 3.9: Use of command Surface from Sketch	21
Figure 3.10: Division of region of body	21
Figure 3.11: Region of division.....	22
Figure 3.12: Division of upper portion of body	22
Figure 3.13: Input values for division	23
Figure 3.14: Example of Mesh	23
Figure 3.15: Demonstration of different sizes of mesh in 2D	24
Figure 3.16: Curvilinear grids	25
Figure 3.17: Unstructured grids.....	25
Figure 3.18: Graphical representation of y^+ value and the x values obtained in an experiment	27
Figure 3.19: Mesh Domain	28
Figure 3.20: Selection of 7 edges	29
Figure 3.21: Boundary layer thickness selection.....	29

Figure 3.22: Selection of Method command	30
Figure 3.23: Selection of Triangle method for mesh.....	30
Figure 3.24: Division of body in different parts.....	31
Figure 3.25: Final Mesh	33
Figure 3.26: Final Mesh zoom-in view	33
Figure 3.27: Nodes and elements demonstration	34
Figure 3.28: Nodes and elements value came from ANSYS	34
Figure 3.29: Using Named Selection command.....	35
Figure 3.30: Name of different portions of Ahmed body.....	35
Figure 3.31: Fluent launcher.....	36
Figure 3.32: Selection of transient time	37
Figure 3.33: Selection of viscous model	38
Figure 3.34: Display of values taken for k-epsilon model	39
Figure 3.35: Selecting inlet conditions.....	40
Figure 3.36: Selecting velocity value	41
Figure 3.37: Selecting area and length	42
Figure 3.38: Selection of Solution Method	43
Figure 3.39: Display of Run calculation.....	46
Figure 3.40: Display of number of iterations against time.....	47
Figure 4.1: Display of reports after running the results.....	48
Figure 4.2: Contours for pressure and velocity profiles	49
Figure 4.3: Display of drag force after simulation	50
Figure 4.4: Pressure profile for 20°angle	50
Figure 4.5: Velocity profile for 20°angle	51
Figure 4.6: Pressure profile for 0°angle	52

Figure 4.7: Velocity profile for 0°angle	52
Figure 4.8: Pressure profile for 40°angle	53
Figure 4.9: Velocity profile for 40°angle	53
Figure 4.10: Pressure profile for 60°angle	54
Figure 4.11: Velocity profile for 60°angle	54
Figure 4.12: Pressure profile for 80°angle	55
Figure 4.13: Velocity profile for 80°angle	55
Figure 4.14: Graph of experimental results of drag coefficient against different yaw angles	57
Figure 4.15: Graph of present findings of drag coefficient against different yaw angles ..	57
Figure 4.16: Comparison of both findings	58
Figure 4.17: Graph of experimental result of drag coefficient and Reynolds number	59
Figure 4.18: Graph of present result of drag coefficient and Reynolds number	60

LIST OF SYMBOLS

L Length of the body, m

q Heat flux, $\text{W}\cdot\text{m}^{-2}$

t Time, min

u Velocity along x-axis, m/s

v Velocity along x-axis, m/s

w Velocity along x-axis, m/s

x Direction along x-axis

y Direction along y-axis

y Distance to the adjacent wall

z Direction along z-axis

Density of fluid, kg/m^3

Shear stress, Pa

Kinematic viscosity, m^2/s

μ Dynamic viscosity, Pa.s

Re Reynolds Number

C_f Skin friction coefficient

C_d Drag coefficient

LIST OF ABBREVIATIONS

ANSYS	Analysis System
CFD	Computational Fluid Dynamics
DES	Detached Eddy Simulation
LES	Large Eddy Simulation
PANS	Partial Average Navier-Stokes
PISO	Pressure-Implicit with Splitting of Operations
PSPG	Pressure Stabilizing Petrov-Galerkin
RANS	Reynolds Averaged Navier Stokes
SGS	Sub-Grid Scale
SUPPG	Upwind Petrov-Galerkin
TDMA	Tri-Diagonal Matrix Algorithm
WHO	World Health Organization

CHAPTER 1

INTRODUCTION

1.1 Automotive Industry

It was observed that there is a rapid change in atmosphere that is noticed because the earth's temperature is increasing rapidly. The value comes out to be 0.85 and for the cold areas, the snow falls has declined by 10%.

The reason behind this is the air pollution that is caused by the vehicles, waste processing industries as per the report of WHO (World Health Organization) due to which problems like cancer, cardiovascular occurs.

For this, (Ahmed S., 1984) has done some experiments in a wind tunnel to test the wake formation. Also, he used a bluff body in order to identify the flow characteristics and forces around the body. The results shows that 85% of the drag is due to the force that is produced at the back end.

1.2 Ahmed Body

Ahmed body is considered to be the benchmark for all the automotive industry. It was initiated back in 1984 by S. R. Ahmed with the findings from an article "Some Salient Feature of the Time-Averaged Wake". About the geometry, it consists of length 1.044 meters, height of 0.288 meters having slant angle that has certain range from 0° to 90° .

The model was presented by (Ahmed et al., 1984). He used several type of data in different locations mainly wind tunnel. After performing a lot of practical demonstrations, drag forces were calculated that is inconsistent (Chong et al., 1990; Serre et al., 2013). In addition to this, (Le Good and Gerry, 2004) used another type of car for this experiment.

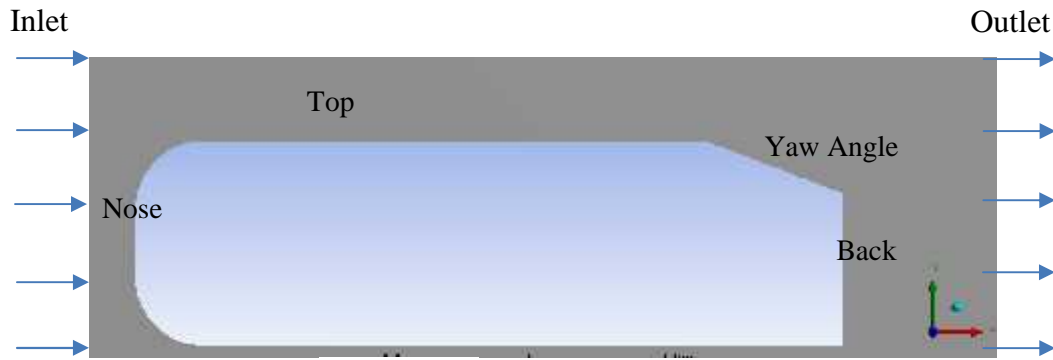


Figure 1.1: Ahmed body model representation in 2D

Now, for CFD analysis, lots of methods have been adopted. Kuzmin, (2010), suggested the CFD analysis. There are lots of methods adopted with different type of vehicles (Smith, 2008) but Ahmed body seems to be the benchmark for CFD analysis (Davis, 2015).

According to Thabet and Thabit (2008), CFD analysis is done in order to find the value of coefficients and the flow properties with the available data.

1.3 Research Aim

The purpose of the research is to examine the Ahmed body for different yaw angles ranging from 0° to 80° through CFD analysis and determine the flow characteristics as a function of Reynolds number and drag coefficient. Also, compare the results with the experimental data that has been done previously by using different Reynolds numbers. Also, to have a comparison of the Reynolds number with the drag coefficient in order to find the difference between the experimental data and the CFD analysis.

1.4 Thesis Outline

Chapter one includes the introduction about the automotive industry and the need of Ahmed body in the industry. Also, the aim behind the research is to incorporate different yaw angles to make a comparison with the experimental setup. Chapter two involves description of Ahmed body along with the literature review that consists of the work that is been done previously. In addition to this, there is theory related to CFD analysis, drag coefficient, Continuity equation, N-S equation, Reynolds Number, Skin friction coefficient, wall shear stress, friction velocity, wall database, yaw angle.

Chapter three comprises of methods adopted for CFD analysis. Chapter four includes the result section in which the values are obtained from the applied method and Chapter five demonstrates conclusion that shows the summary of the outcomes obtained through CFD analysis.

CHAPTER 2

LITERATURE REVIEW AND THESIS

2.1 Literature Review

Initially Ahmed body was designed for investigating impact of slant angle along drag force despite of yaw angles but yaw angles were investigated on a small scale (Ahmed et al, 1984). After changing from 2D to 3D, drag forces were observed in the middle of 12.5° and 30° because of low pressure state (Howard and Pourquie, 2002). By using different angles, we observe different studies within the body (Krajnovic et al, 2011, 2012)

For CFD, Reynolds Averaged Navier Stokes (RANS) method has been adopted (Han, 1989; Guilmineau, 2008) and also Large-Eddy Simulation (LES) has been implemented on Ahmed body (Hinterberger et al, Krajnovic and Daridson, 2005 a,b).

According to Serre et al, (2013), it includes the method of Reynolds Averaged Navier Stokes (RANS) with another three more methods that can be used for further calculation that includes Detached Eddy Simulation (DES), Sub-grid Scale (SGS) and LES simulation.

Franck et al., (2009) utilizes two schemes namely Upwind Petrov-Galerkin (SUPPG) schemes and Pressure Stabilizing Petrov-Galerkin (PSPG) in order to identify pressure and velocity profiles with the angle 12.5° by using LES simulation.

There is a new method that is introduced with the procedure of PANS (Partial Average Navier-Stokes) equations by Mirzaei et al, (2015) to gather the flow characteristics.

Also, there are CFD simulations that can be verified by using the experimental setup and comparing values of both and analyze drag coefficients. The first drag coefficient using Reynolds number (Re) by Meile et al, (2011) through using FLUENT.

Again Conan et al, (2011) used different angles to calculate different values of drag forces. Now, divergence of flow was observed by making a comparison of sharp and rounded which is at the joint of roof and rear slope while optimizing a zero yaw angle. It was

observed that the Reynolds number incline upwards as drag coefficient seems to go down. (Wang et al., 2013)

After this, we will look into yaw angle impact on Ahmed body. Initially, yaw angle was investigated at zero degree to analyze cross wind impact that shows that the angle was in between -3° and 3° by the rise in drag co-efficient (Bayraktar et al., 2001)

Not long ago, Chometon et al., (2004) used another body instead of Ahmed body to fine effect of yaw angle. Carey et al, (2006) used yaw angle of 12° keeping the same body. But after some time there was another model called Willy model was used to investigate the forces that demonstrates powerful vertices on back side (Golhke et al, 2007, 2009)

There is a new software that is ISIS-CFD is used by Gurlmineau et al, (2013) for analyzing different angles but found out the inclination of yaw angles from 0° to 30° . Volpe et al, (2014) has practically worked on the bends of wake structures at a side on the crosswind.

Millan and Makela, (2016) analyze yaw angles from 0° to 90° by using experimental setup in a wind tunnel to describe drag co-efficient and the flow characteristics.

The present study demonstrates utilization of yaw angles from 0° to 80° using CFD analysis and compare the results from the experimental results and determine drag co-efficient and flow visualization in terms of Reynolds number that is obtained analyzing the CFD analysis. For this, we have used the standard k-epsilon method in order to analyze the model and have the desired results with velocity and pressure flow.

2.2 CFD Analysis

CFD includes computer based simulations that includes problems regarding automotive, power plant and turbines etc. in which certain boundary conditions are applied in order to analyze the problems as per requirements of a user that includes heat transfer and fluid particles problems. The method is very useful in industrial and non-industrial applications.

The reason why CFD is most preferred as compared to other computer software is that it is user friendly and easy to use. It gives a lot of options including calculations of stresses and strains, forces and volumes, velocity and pressure distributions etc. So, it takes less time on

order to solve a problem as compared to other software and also provides precise and accurate values so that it can be compared with the experimental data.

2.3 Components of CFD

CFD has three major components that is listed below:

- Pre-Processor
- A Solver
- Post-Processor

Now, we will go through all these one by one.

2.3.1 Pre-Processor

It is the initial step in order to analyze a problem. The main objective of this method is to transfer the data into a form which is user friendly and can easily be solved by the users. It involves first the definition of computational domain in which we have to select the domain in which geometry of object being drawn. After that, we divide the domain into smaller cells or groups in order to have accurate results. After finishing this, we select the type of phenomena that needs to be modelled. Then we have to specify the fluid properties that which type of fluid we have to select like air or water. At the end, we have to apply boundary conditions that are different for different cases.

In this process, we have to closely consider the nodes in each of the cells as it will describe the precision of the results that are obtained for solving the problem. The time required to have a solution and the precision of the end results is entirely dependent on the dimension of grid. This procedure is entirely dependent on the end user which is analyzing the problem and grid can be change as per requirements.

In CFD, work domain and grid analysis is the main components in the pre-processor domain. In industries, more than 50% of time is used in analyzing these two components. Also, if we use a updated version of pre-processor, it give access into special physical and chemical procedures that provides the precise results without manually inserting equations and reduce the time of the end user

2.3.2 Solver

Solver consists of mainly three components namely:

1. Finite difference
2. Finite element
3. Spectral method

But the main component that is normally adopted is the finite volume procedure that comprises of certain CFD codes like CFX/ ANSYS, FLUENT, PHOENICS and STAR-CD.

The numerical method consists of three steps. Initially, control volume separates finite volume from different CFD approaches. Basically it converts the properties in the engineering form that can be easily understood by the engineer using the CFD program like equations, formulae's. It also considers the balance of the equation that shows the trend of inclining upwards or downwards.

Most commonly procedures that are commonly used in the solver domain are Tri-Diagonal Matrix Algorithm (TDMA), line-by-line solver and SIMPLE algorithm that are best converters for the measurement of pressure and velocity.

2.3.3 Post-Processor

In recent times, there are lots of modifications has been done in this section as per the engineer's requirements. Now, CFD includes varieties in the graphics section that comprises of:

- Geometry of domain and grid display
- Vector plots
- Contour areas
- 2D and 3D surface
- Color PostScript output

2.4 Advantages of CFD Analysis

1. CFD program is not expensive as compared to other software
2. It does not consume a lot of time for execution of program
3. It helps to easily convert any sort of problem into the physical condition
4. CFD allows a user to have full access on the process
5. CFD is user friendly and allows to work on 3D model as well
6. Large complex systems can be analyzed easily
7. It gives precise results and eliminating the irrelevant data if necessary
8. The chances of error is minimum using CFD analysis

2.5 Disadvantages of CFD Analysis

1. The model is entirely dependent on time
2. Solution obtained is as precise as the physical model is constructed
3. There are round-off errors because of word size limitations
4. Also, chance of truncation error occurs that can be eliminated through mesh refinement

2.6 Drag Coefficient

The drag coefficient is defined as the friction that is applied by an object. It can differ due to certain reasons like the velocity and direction of flow, shape and size of object and viscosity and density of the fluid. The optimum condition is that the drag coefficient should be as minimum as possible because the minimum is the drag coefficient, the efficient will be the car. But it should not be totally eliminated as it can increase chances of car accidents.

Normally, drag coefficient depends on Reynolds number and certain other factors. In order to minimize drag coefficient, there are various methods to edit the car model like eliminate roof rack, mud flaps, radio antenna and spoilers. Also, drag coefficient can be enhanced by the fender skirts and wheel covers.

Before start the mathematical calculations, let's see the boundary conditions that are used in this article

2.7 Boundary Conditions

In order to derive certain equations, we need to look into the boundary conditions that are used to simplify the equation as per the requirements of this case:

-) No heat transfer between the flow and geometry
-) No slip condition
-) Flow will be incompressible ($\beta = 0$)

2.8 Continuity Equation

The continuity equation demonstrates movements of few entities. It demonstrates the physical phenomena that are conserved including mass, energy, momentum and remaining entities.

Now, we will take example of conservation of mass and derive equation for this

2.8.1 Conservation of Mass

We will take the mass flow and the flow inside and outside of the body. We will combine the mass flow in and out that is shown in Figure 2.1

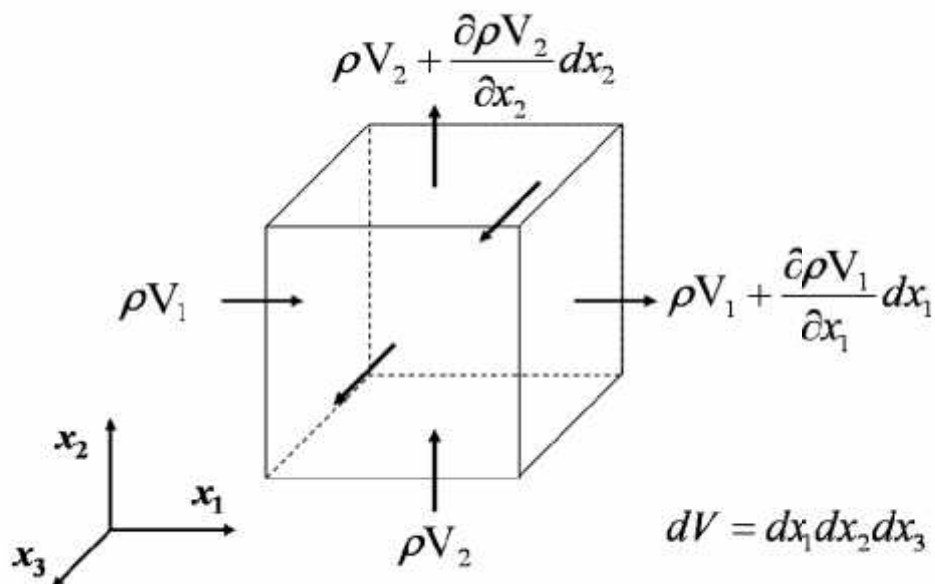


Figure 2.1: Conservation of mass in and out of a body

After solving the mass flow in and out, equation comes out to be

$$\frac{\partial \rho}{\partial x} + \frac{\partial \rho u_x}{\partial x} + \frac{\partial \rho u_y}{\partial y} + \frac{\partial \rho u_z}{\partial z} = 0 \quad (2.1)$$

For incompressible flow,

$$\frac{\partial u_x}{\partial x} + \frac{\partial u_y}{\partial y} + \frac{\partial u_z}{\partial z} = 0 \quad (2.2)$$

This is the final equation that will be used as per the boundary conditions where u, v and z are velocities along x, y and z axis.

Where,

ρ is density

u is the velocity

2.9 Navier Stokes Equation

It is a partial differential equation that consists of incompressible flows. This equation is applicable in measuring water flow in a pipe, air flow across a wing and especially in the composition of aircrafts and cars.

Navier stokes equation for 3 dimensional flow neglecting higher order terms is

For X-Momentum

$$\frac{\partial(\rho u)}{\partial t} + \frac{\partial(\rho u^2)}{\partial x} + \frac{\partial(\rho u v)}{\partial y} + \frac{\partial(\rho u w)}{\partial z} = -\frac{\partial p}{\partial x} + \frac{1}{Re} \left[\frac{\partial \tau_x}{\partial x} + \frac{\partial \tau_{xy}}{\partial y} + \frac{\partial \tau_{xz}}{\partial z} \right] \quad (2.3)$$

For Y-Momentum

$$\frac{\partial(\rho v)}{\partial t} + \frac{\partial(\rho u v)}{\partial x} + \frac{\partial(\rho v^2)}{\partial y} + \frac{\partial(\rho v w)}{\partial z} = -\frac{\partial p}{\partial y} + \frac{1}{Re} \left[\frac{\partial \tau_{xy}}{\partial x} + \frac{\partial \tau_y}{\partial y} + \frac{\partial \tau_{yz}}{\partial z} \right] \quad (2.4)$$

For Z-Momentum

$$\frac{\partial(\rho w)}{\partial t} + \frac{\partial(\rho u)}{\partial x} + \frac{\partial(\rho v)}{\partial y} + \frac{\partial(\rho w^2)}{\partial z} = -\frac{\partial p}{\partial z} + \frac{1}{Re} \left[\frac{\partial \tau_x}{\partial x} + \frac{\partial \tau_y}{\partial y} + \frac{\partial \tau_z}{\partial z} \right] \quad (2.5)$$

But for this case, after we use the given boundary conditions, the Navier stokes equation will become

For X-Momentum

$$\frac{\partial(\rho u)}{\partial t} + V(\rho u) = -\frac{\partial p}{\partial x} + \frac{\partial}{\partial x} + \frac{\partial}{\partial y} + \frac{\partial}{\partial z} + \rho \quad (2.6)$$

For Y-Momentum

$$\frac{\partial(\rho v)}{\partial t} + V(\rho v) = -\frac{\partial p}{\partial y} + \frac{\partial}{\partial x} + \frac{\partial}{\partial y} + \frac{\partial}{\partial z} + \rho \quad (2.7)$$

For Z-Momentum

$$\frac{\partial(\rho w)}{\partial t} + V(\rho w) = -\frac{\partial p}{\partial z} + \frac{\partial}{\partial x} + \frac{\partial}{\partial y} + \frac{\partial}{\partial z} + \rho \quad (2.8)$$

Where,

V is Laplace operator

ρ is density

τ is shear stress

t is time

ν is viscosity

f is Buoyancy Force

2.10 Skin Friction Coefficient

Skin friction determines the region of shear flow near the boundary layer. There are different region in which viscosity occurs like viscous sub-layer, buffer layer, inertial layer and wake function.

Skin friction coefficient is demonstrated as

$$C_f = [2\log_{10} (Re_x) - 0.65]^{-2.3} \quad (2.9)$$

Where,

Re_x is Reynolds number

C_f is Skin Friction coefficient

2.11 Wall Shear Stress

It is termed as shear stress near the wall of the object. As per the flow, it is considered to be slow at the corners and fast at the center. Then, a parabolic shape is observed which is due to laminar flow that is because of the friction between fluid and wall. A force is produced because of the friction called wall shear stress

It is stated as

$$\tau_w = C_f \times \frac{1}{2} \rho u^2 \quad (2.10)$$

Where,

ρ is the density of fluid

u is the velocity of object

C_f is the skin friction coefficient

2.12 Friction Velocity

It is also called shear velocity. It is helpful in analyzing the velocities between actual velocity and the velocity flowing in a stream.

It is defined as,

$$u^* = \sqrt{\frac{\tau}{\rho}} \quad (2.11)$$

Where,

τ is shear stress

ρ is the density of fluid

2.13 Wall Distance

Wall distance for a particular case is mentioned as,

$$y^+ = \frac{\mu y^+}{\rho u^*} \quad (2.12)$$

u^* is friction velocity

y is distance to the adjacent wall

μ is viscosity

ρ is the density of fluid

y^+ have no dimensions and utilized in CFD analysis to determine mesh refinement for a specified flow. y^+ has certain values and has certain ranges for different cases. We will consider the viscous effects that has different values for different regions like

-) $y^+ < 5$ for viscous sub-layer
-) $5 < y^+ < 30$ for buffer layer
-) $y^+ > 30$ to 60 for fully turbulent region

For larger value of y^+ , the grid size should be minimized to have a precise result.

CHAPTER 3

METHODOLOGY

In this section we will discuss about the method that is being adopted to obtain the desired results. For the Ahmed body to be analyzed, there are lots of software available but for this case we will use Ansys. First of all we will define geometry as per specified before in the article and then we will apply certain operations in order to get the results.

For this, we have divided this into four steps:

-) Geometry
-) Meshing
-) Setup
-) Results and Discussions

So first we will describe geometry and change angles from 0° to 80° with interval of 20° . And after this we will find out the boundary layer thickness through which we can describe the mesh of the object through “Number of Division” method and after completing mesh, boundary conditions will be inserted in order to define what are the desired results and after finishing this, desired results would be attained and velocity and pressure profiles would be compared at certain angles.

So, let start with the first step of setup,

3.1 Geometry

The first thing that should be done is starting Ansys. In this thesis, we have used latest version of Ansys 17.2.

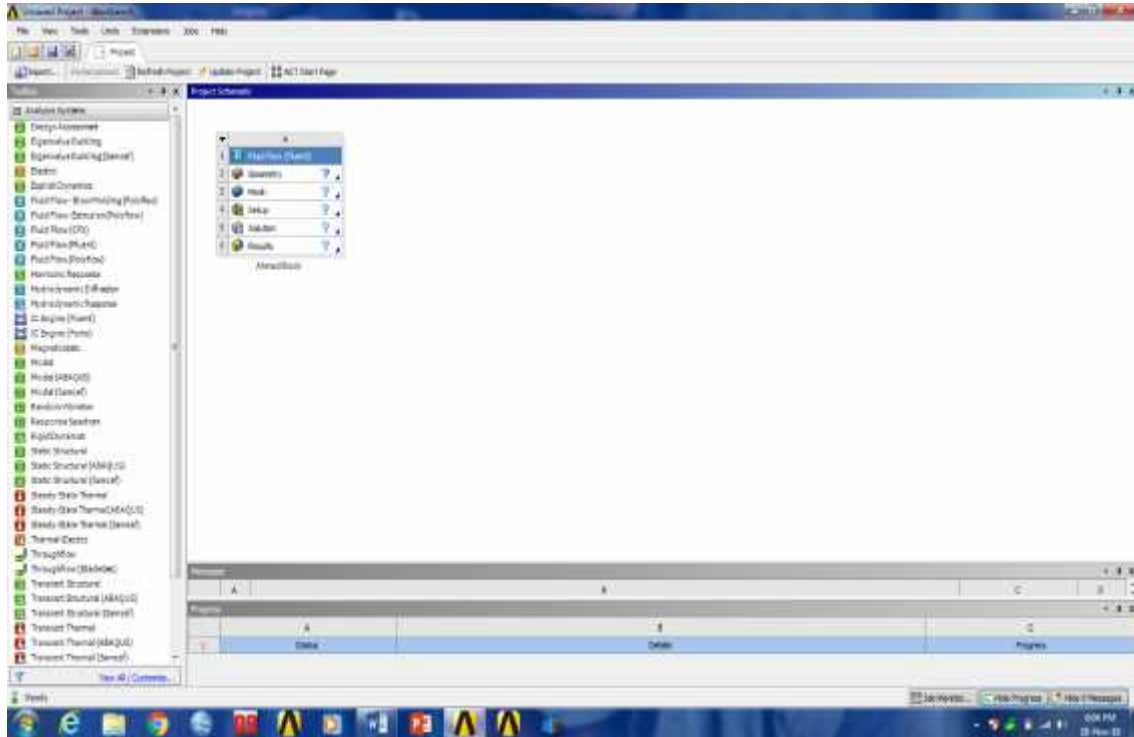


Figure 3.1: Ansys workbench for analysis of problem

After opening the workbench, right click on geometry and then click New Design Model geometry as shown in below Figure 3.2

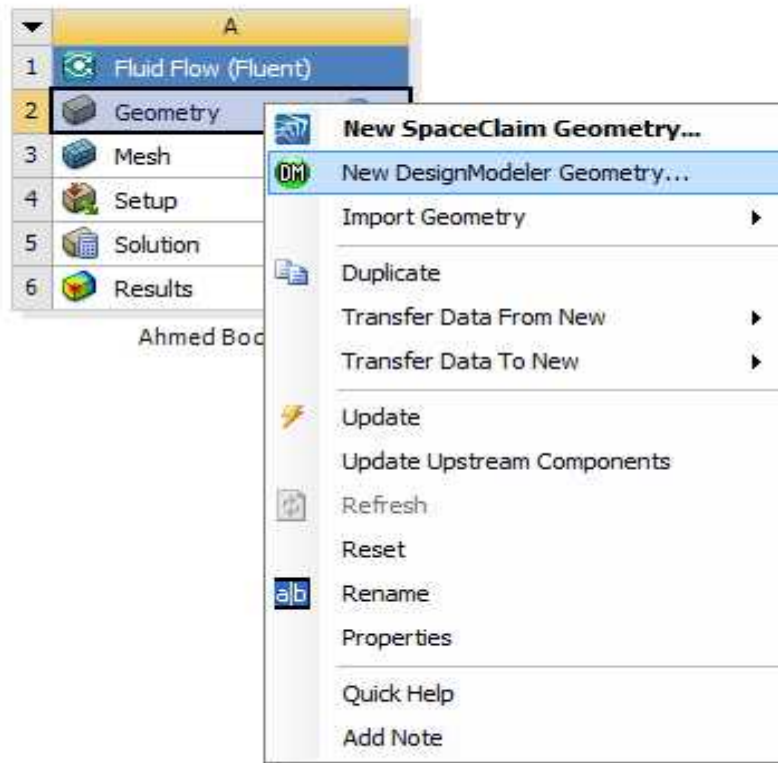


Figure 3.2: Design-Modeler Geometry domain

After click on the icon, a separate window will appear that includes Design Modeler in which geometry is prepared.

After that select XY plane and select sketching option in order to draw the geometry shown in Figure 3.3

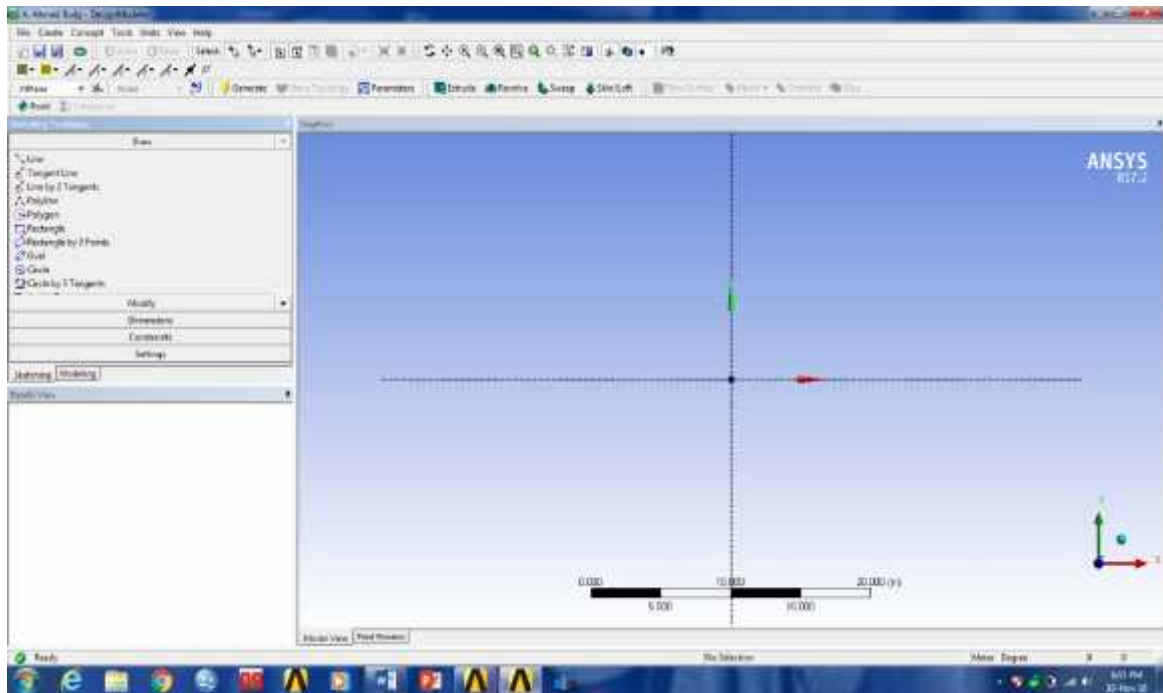


Figure 3.3: Selection of XY Plane

After that select triangle and draw a triangle that shows Ahmed body. As been previously shown, the dimensions of Ahmed body is shown below. But for simulation, we are drawing Ahmed body in 2D so that it can be analyzed easily.

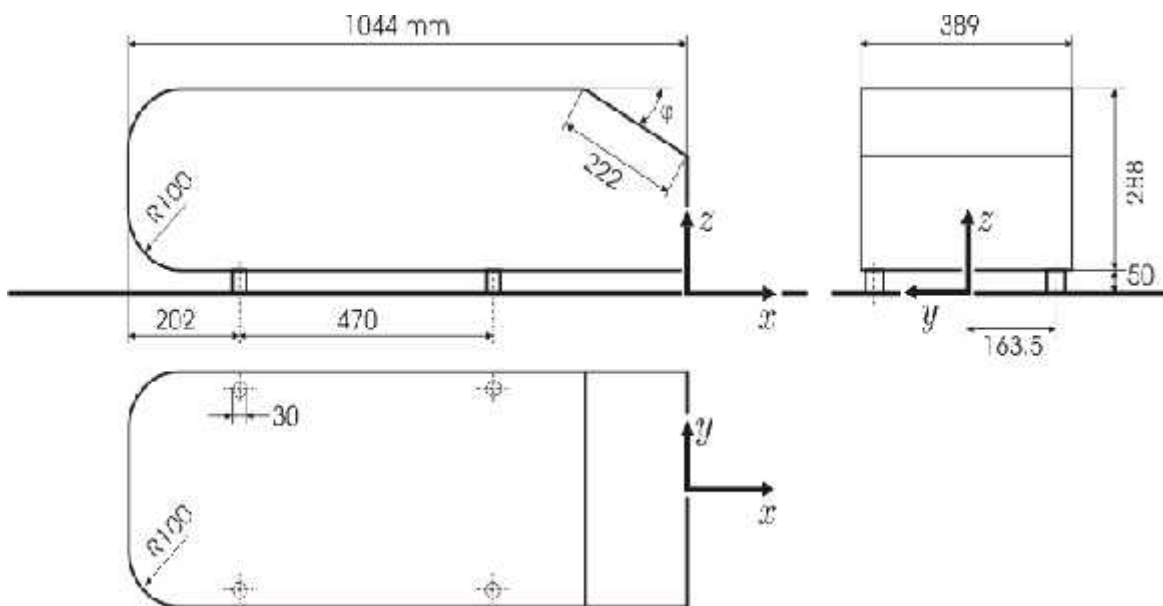


Figure 3.4: Ahmed body dimensions in millimeters

So, we select and draw triangle. We take units in 'm' so the length of body will be 1.044m and height would be 0.288.

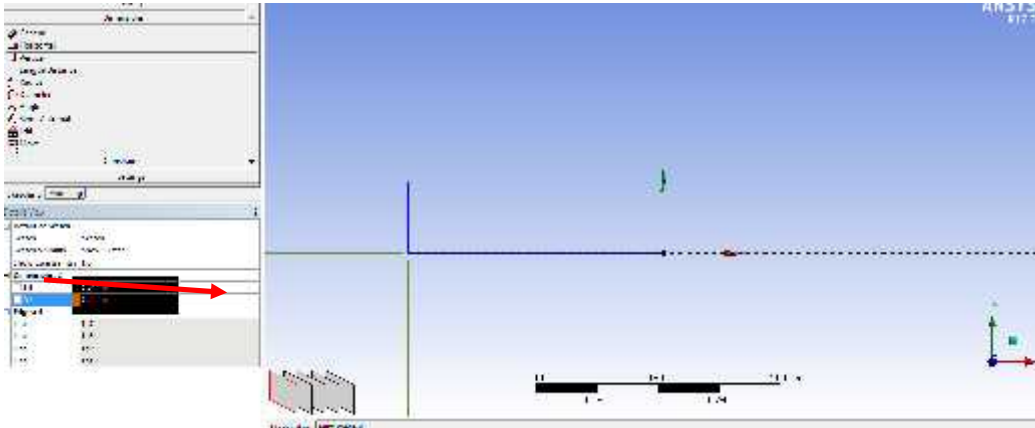
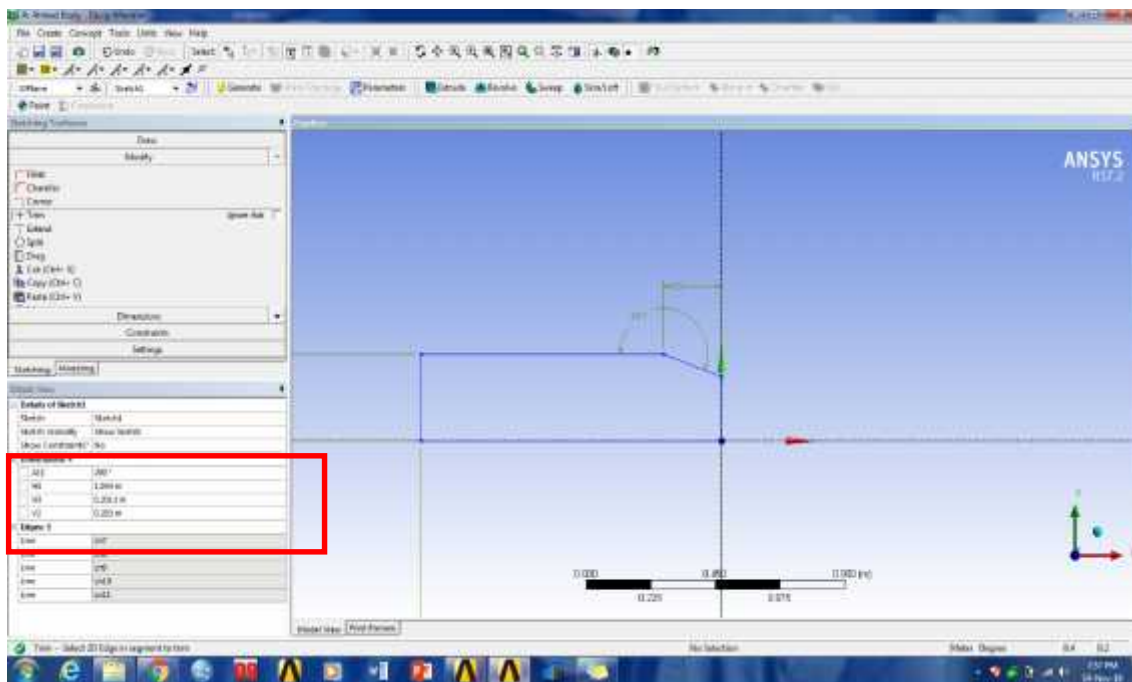


Figure 3.5: Dimension of horizontal and vertical dimensions of body in meter

After this, we will draw a line with a dimension of 0.2012m as shown. Then, we define angle of Ahmed body. In this case, we will take 20° so $180+20=200^\circ$ would be our angle. After defining angle, we will use command of Trim to demonstrate angle of Ahmed body precisely demonstrated in Figure 3.6



Snow Constraints: NO	
Dimensions: 4	
<input type="checkbox"/> A11	200 °
<input type="checkbox"/> H1	1.044 m
<input type="checkbox"/> H3	0.2012 m
<input type="checkbox"/> V2	0.283 m
Edges: 5	

Figure 3.6: Defining yaw angle

After that we use command of “Fillet” in order to have two fillet surfaces with radius of 0.1m has been shown in Figure 3.7

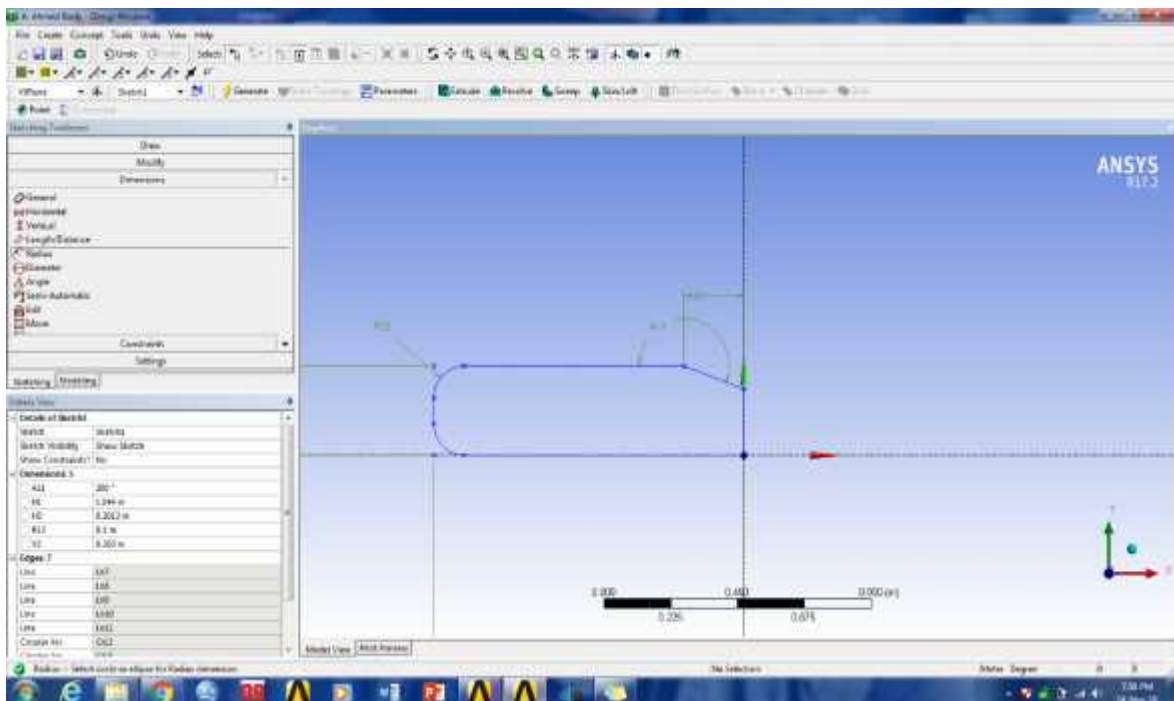
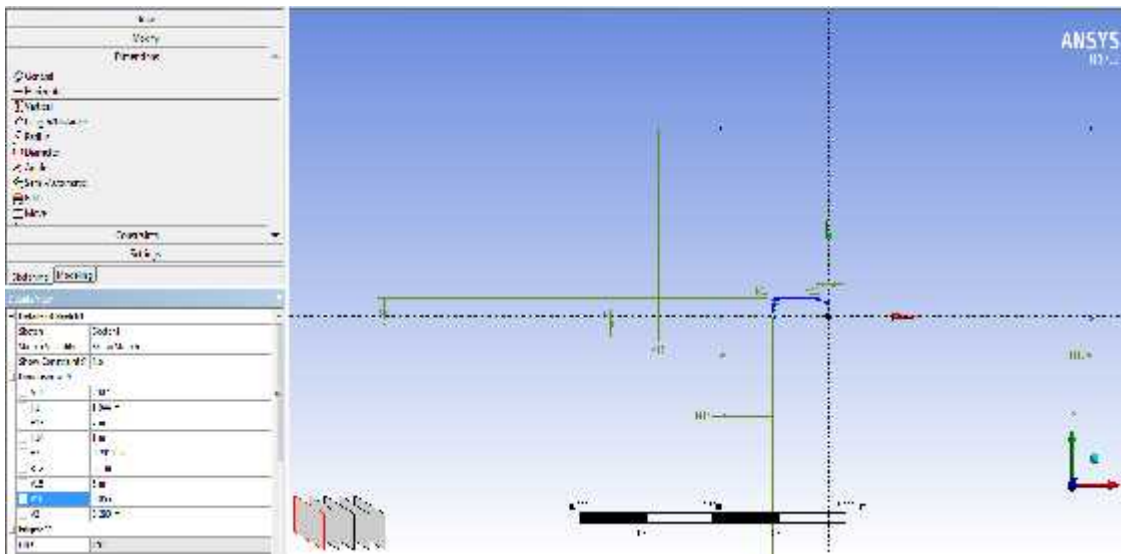


Figure 3.7: Use of commands of Fillet and Trim

After this step, we will enclose Ahmed body in another body in order to simulate and have precise results. Also, we need to define inlet and outlet of the body that will be defined by this body shown in Figure 3.8



<input type="checkbox"/>	A11	200 °
<input type="checkbox"/>	H1	1.044 m
<input type="checkbox"/>	H13	7 m
<input type="checkbox"/>	H14	1 m
<input type="checkbox"/>	H3	0.2012 m
<input type="checkbox"/>	R12	0.1 m
<input type="checkbox"/>	V15	3 m
<input checked="" type="checkbox"/>	V16	0.05 m
<input type="checkbox"/>	V2	0.283 m

Edges: 11

Figure 3.8: All dimensions used in body

After defining another geometry, we will use command of “Surface from Sketch” in order to fill in the surface that will help in analyzing flow around the whole body. And we will select the whole body except Ahmed body for analysis.

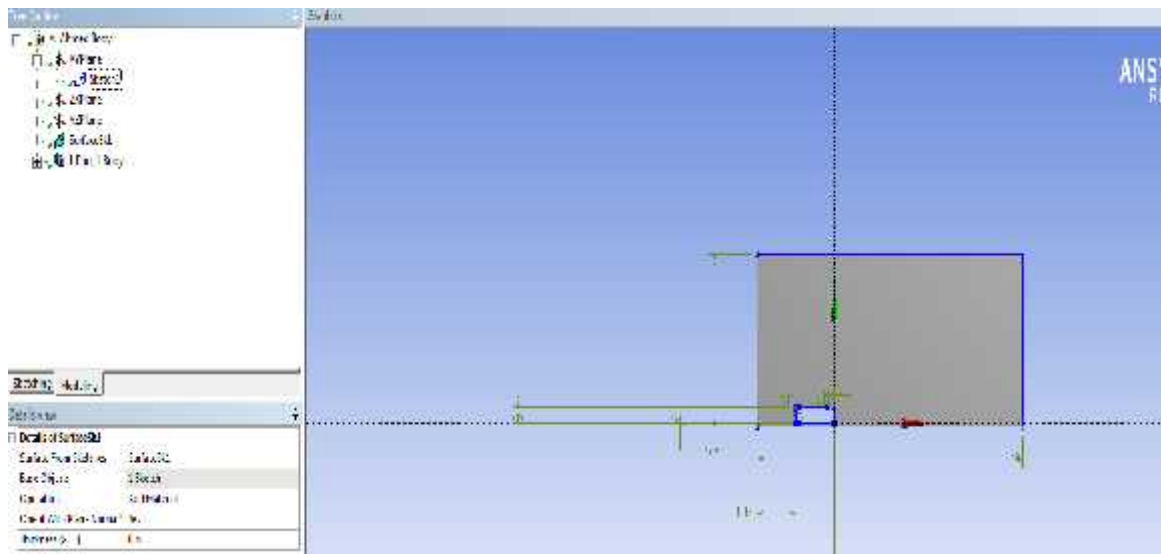


Figure 3.9: Use of command Surface from Sketch

Then, we will again divide the whole body in different regions in order to have precise results. We will divide the body so that we can only closely look around Ahmed body. We will draw lines across Ahmed body as shown in Figure 3.10

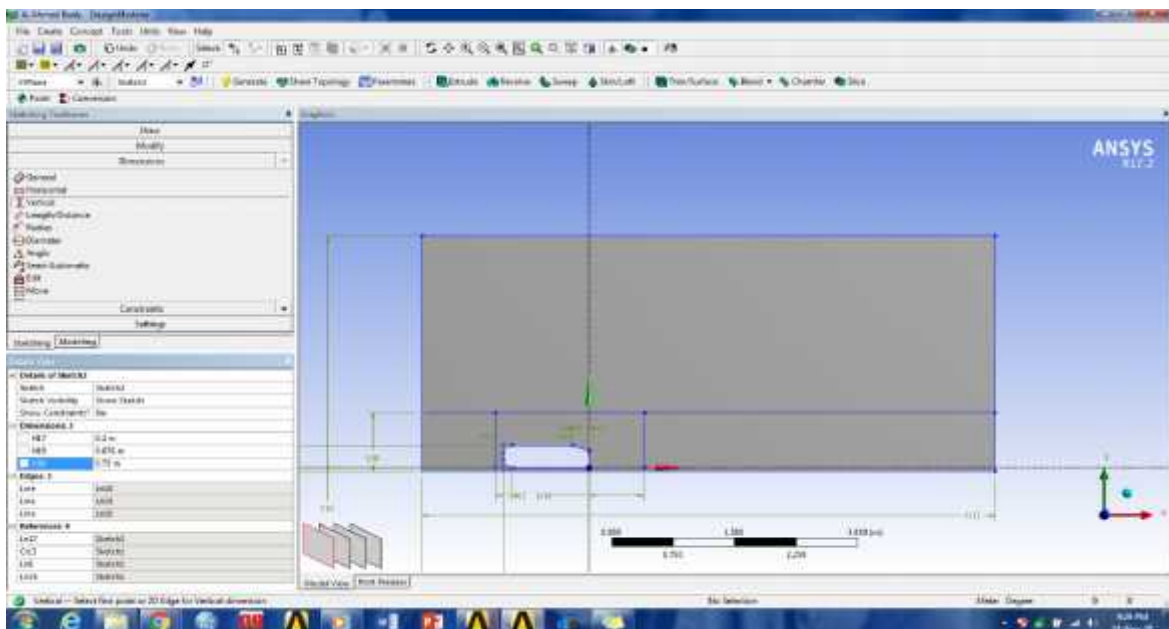


Figure 3.10: Division of region of body

Then, we will again have to separate the Ahmed body from entire body. For this, we will use command of “Face Split”. So, first we will divide upper portion from bottom portion as shown in Figure 3.11

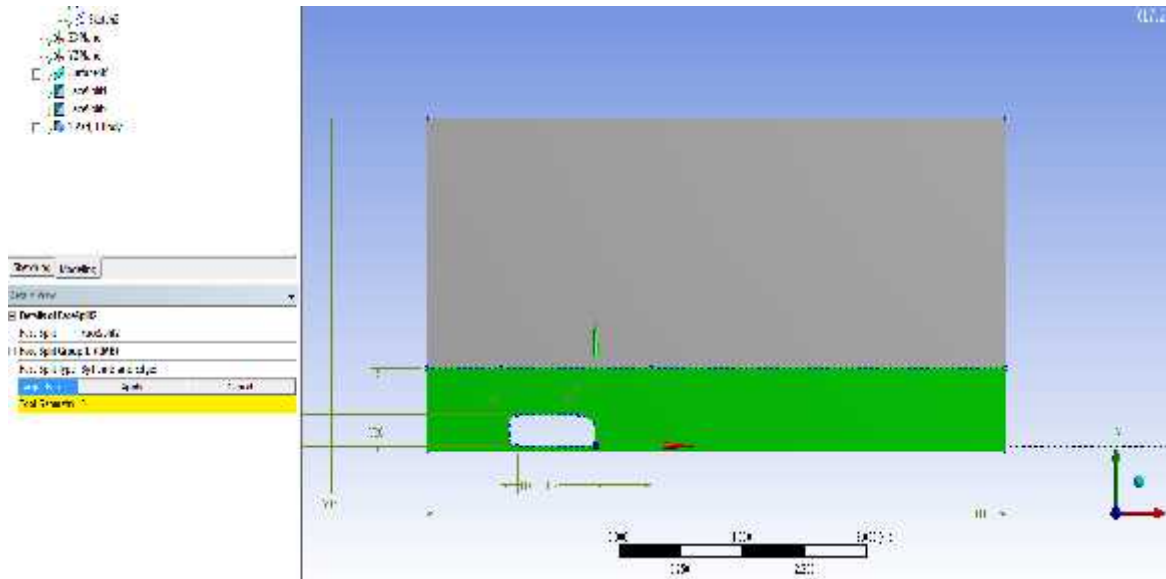


Figure 3.11: Region of division

And again we will do it three times and after that we will get this final result in which we will consider only portion of Ahmed body. After that, we will use command of ‘Edge Split’ so that we split the upper body of Ahmed body in portions as shown in Figure 3.12

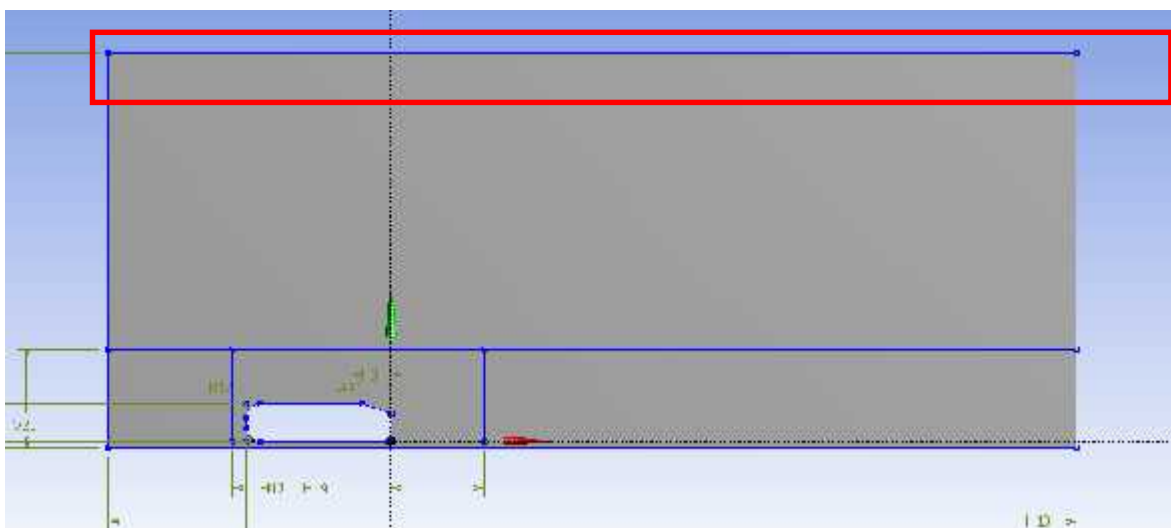


Figure 3.12: Division of upper portion of body

For this, we will use this command two times in which we will use FDI, fraction 0.09955 and 0.265. We get these values through “Dimensions” command in geometry

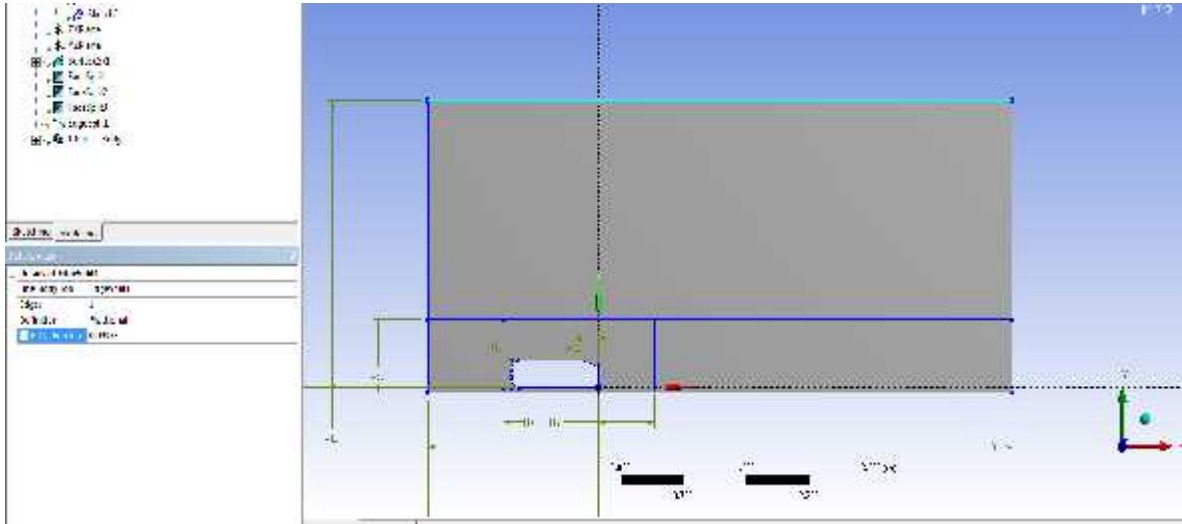


Figure 3.13: Input values for division

3.2 Meshing

Meshing is considered to the division of element into different regions. Mesh is comprises of different types depending on the user’s requirements.

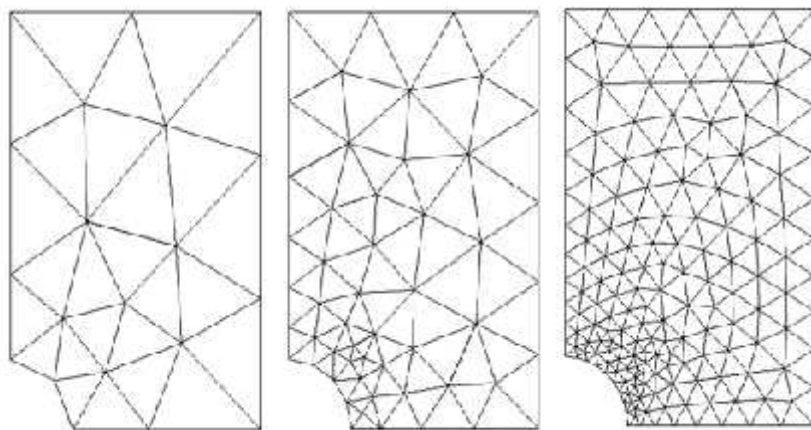


Figure 3.14: Example of Mesh

There are four different shapes in which elements are demonstrated that are namely:

-) Tetrahedral
-) Hexahedral
-) Prismatic
-) Pyramid

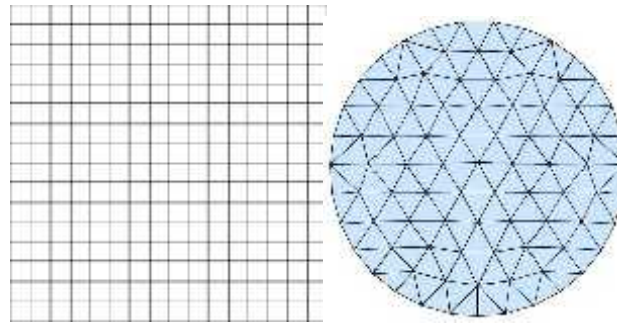


Figure 3.15: Demonstration of different sizes of mesh in 2D

3.2.1 Nodes

Elements that are joined together through nodes, each representing certain vertices that are used for the meshing process.

3.2.2 Division of Grids:

The grids are divided into two types that are structured curvilinear grid arrangement and unstructured grid arrangement.

➤ *Structured Curvilinear Grid Arrangements*

In this type of meshing, there are specified amount of grids that are very close to each other. Their job is to display the flow with an easy appearance. It divides the section into different sub-divisions. These subdivisions are meshed individually and connected with others known as Block structured grid.

It includes two types namely orthogonal curvilinear grids and Non-orthogonal coordinate.

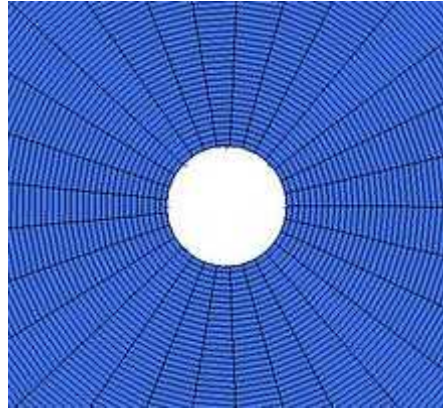


Figure 3.16: Curvilinear grids

➤ *Unstructured Grid Arrangement*

During the analysis of CFD, we use this kind of arrangement because of the more complex geometry. The reason behind using this method is the maximum optimization of the computational domain. For this type, cells are arranged in a shape of block. The benefit of using this type is that you can refine the mesh whenever needed as per requirements. We use hybrid grids because it is a combination of both triangular and quadrilateral elements as shown in below figure.

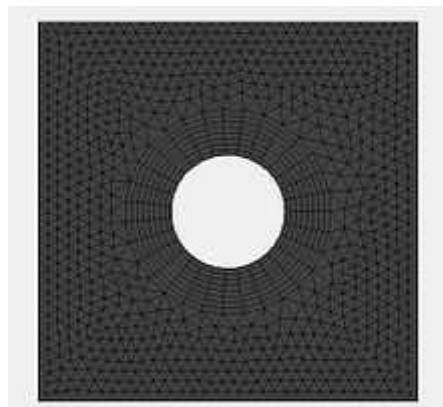


Figure 3.17: Unstructured grids

3.2.3 Calculations for determining Boundary Layer Thickness

First we have to find value of y so that we can have value of boundary layer thickness that will be used for meshing.

➤ *Reynolds Number*

For this case we will take Reynolds number of 6.96×10^5 . (Millon and Makela, 2016)

➤ *Skin Friction Coefficient (Cf)*

$$C_f = [2 \log_{10} (Re_x) - 0.65]^{-2.3} \quad (3.1)$$

$$C_f = [2 \log_{10} (6.96 \times 10^5) - 0.65]^{-2.3} \quad (3.2)$$

$$C_f = 3.99 \times 10^{-3} \quad (3.3)$$

➤ *Wall Shear Stress (τ_w)*

$$\tau_w = C_f \times \frac{1}{2} \rho u^2 \quad (3.4)$$

$$\tau_w = 3.99 \times 10^{-3} \times \frac{1}{2} (1.225)(40)^2 \quad (3.5)$$

$$\tau_w = 3.916 \text{ Pa} \quad (3.6)$$

➤ *Friction Velocity*

$$u^* = \sqrt{\frac{\tau_w}{\rho}} \quad (3.7)$$

$$u^* = \sqrt{\frac{3.9}{1.2}} \quad (3.8)$$

$$u^* = 1.788 \text{ m/s} \quad (3.9)$$

➤ *Wall Distance (y)*

$$y = \frac{\mu y^+}{\rho u^*} \quad (3.10)$$

$$y = \frac{1 \times 1.7 \times 10^{-5}}{1.2 \times 1.7} \quad (3.11)$$

$$y = 8.17 \times 10^6 \text{ m} \quad (3.12)$$

We take y^+ of 1 from (Salim&Cheah, 2009)

In this case, we will take y^+ of value 1. From the article Salim and Cheah (2009), y^+ considers to be 30 for the lower bond and for wall functions and for the wall functions, we take y^+ to be 1 which is the benchmark for this method. For these values, an experiment was performed to analyze the undisturbed flow by Zeiden. Y^+ value differs with different number of cells used for meshing mentioned below:

-) Mesh 1 (3000 cells)
-) Mesh 2 (4000 cells)
-) Mesh 3 (10600 cells)

So, it is shown graphically, values of y^+ against these mesh ranges below in Figure 3.18

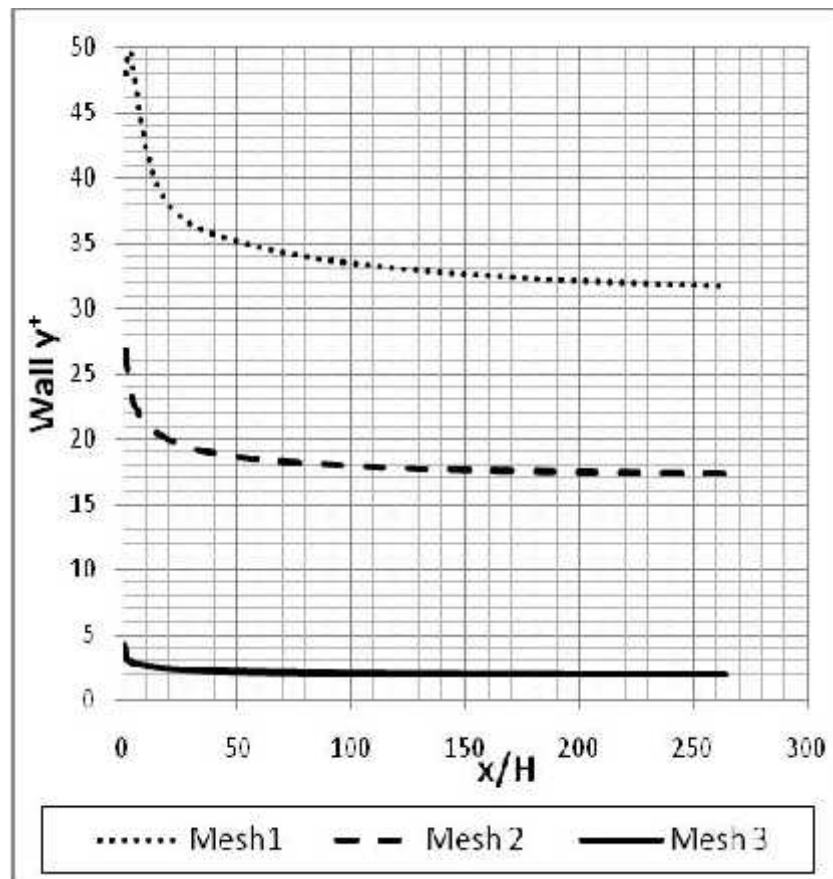


Figure 3.18: Graphical representation of y^+ value and the x values obtained in an experiment

So, we will take boundary layer thickness of 8.17×10^{-6} m. Now we will look into steps of meshing.

First we will look into work domain

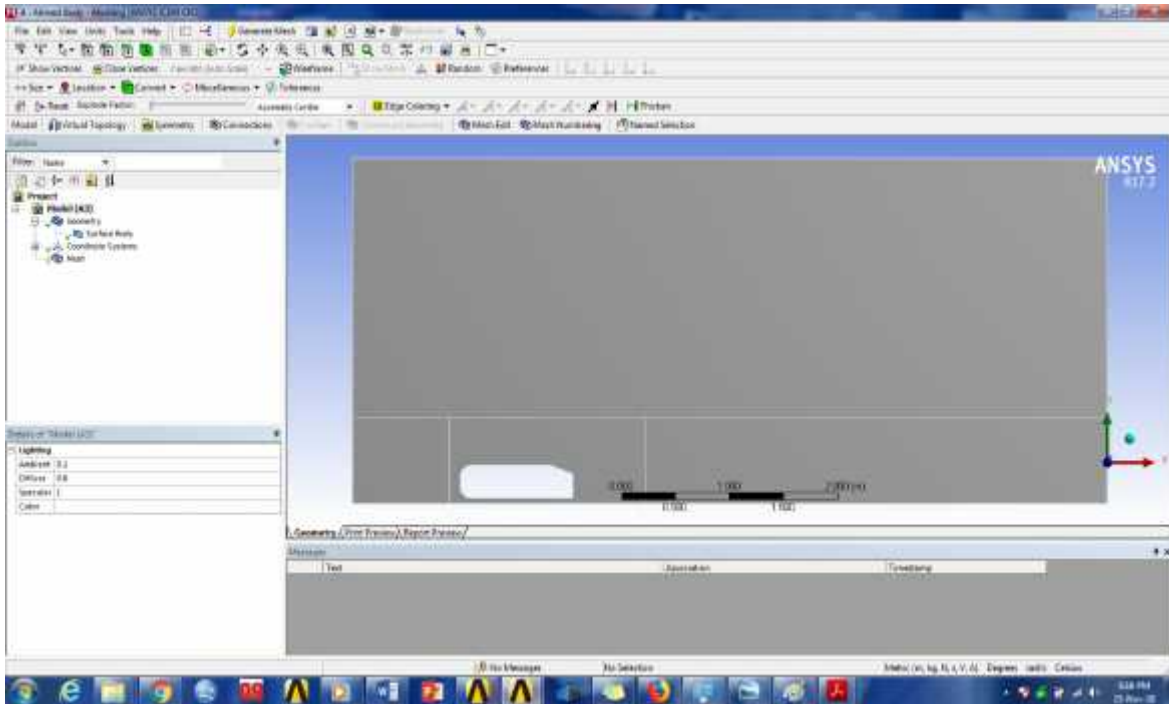


Figure 3.19: Mesh Domain

First, we will define boundary layer thickness so we will use command of “Inflation” and insert first layer thickness by selecting 7 edges of Ahmed body shown in Figure 3.20 and 3.21.

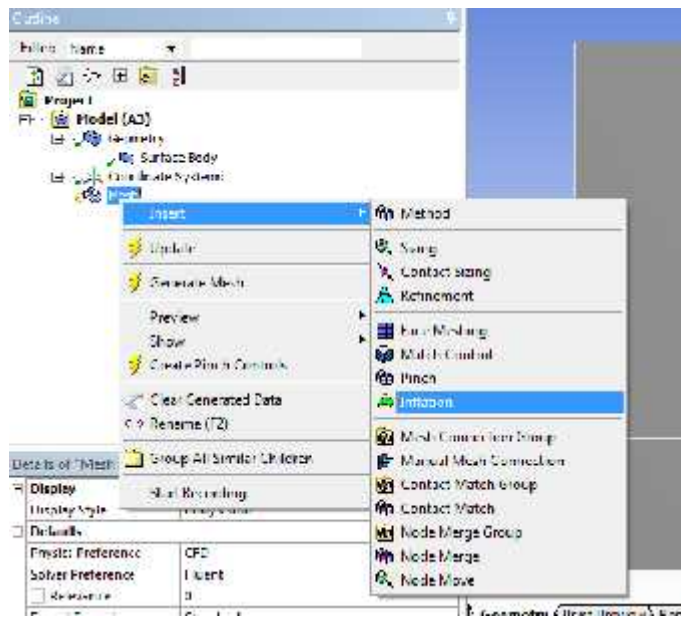


Figure 3.20: Selection of 7 edges

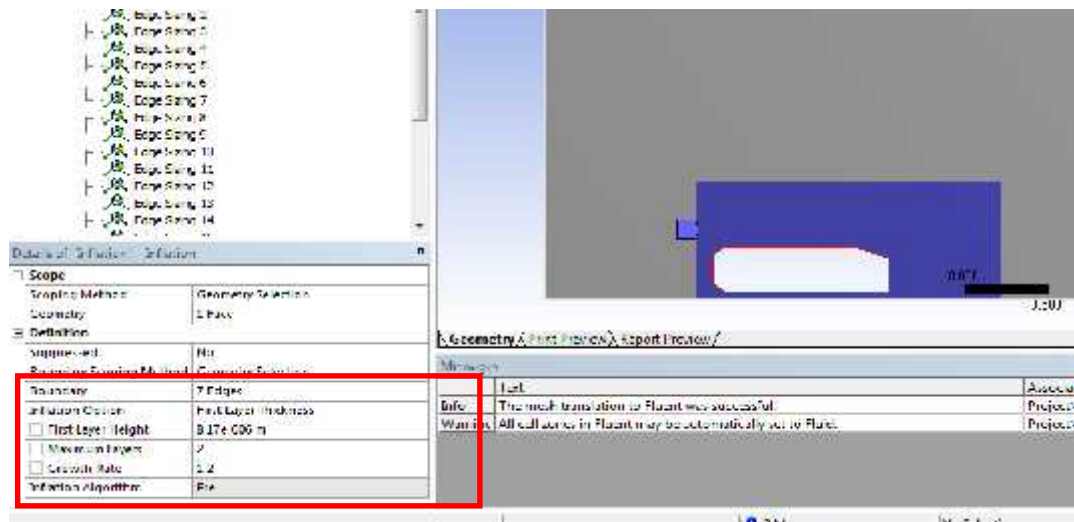


Figure 3.21: Boundary layer thickness selection

Now, we will define the type of mesh. In this article we will use “Triangles” method in order to have simple and refined mesh defined in Figure 3.23

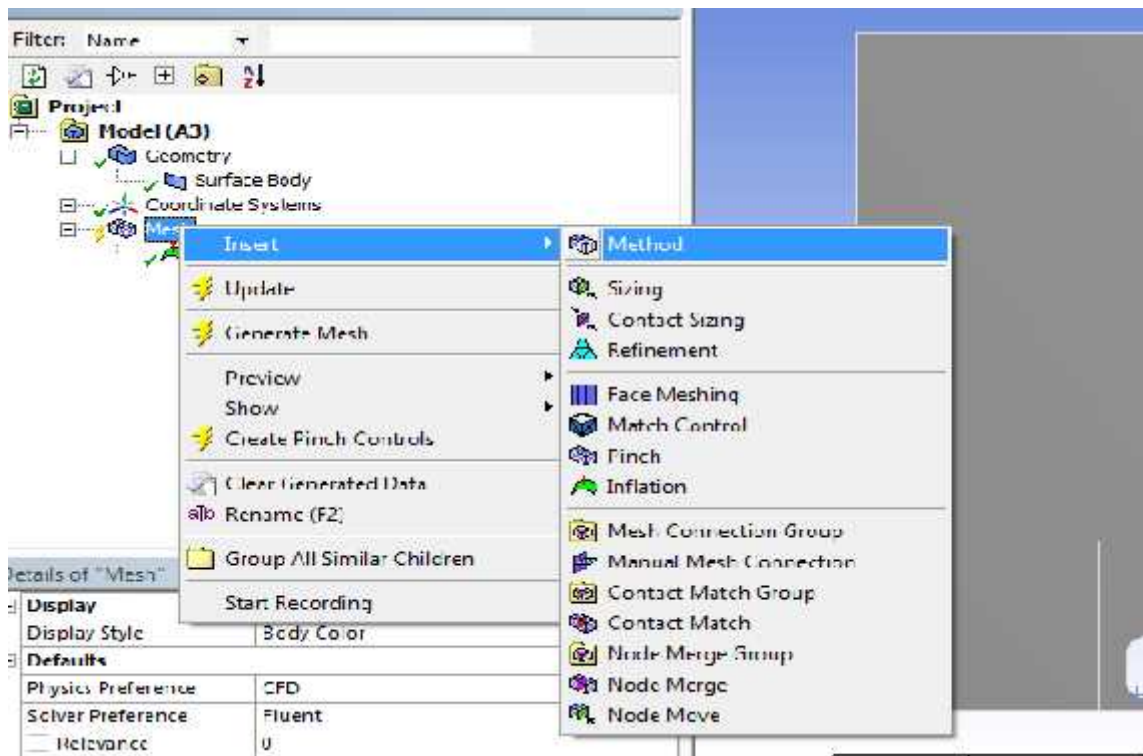


Figure 3.22: Selection of Method command

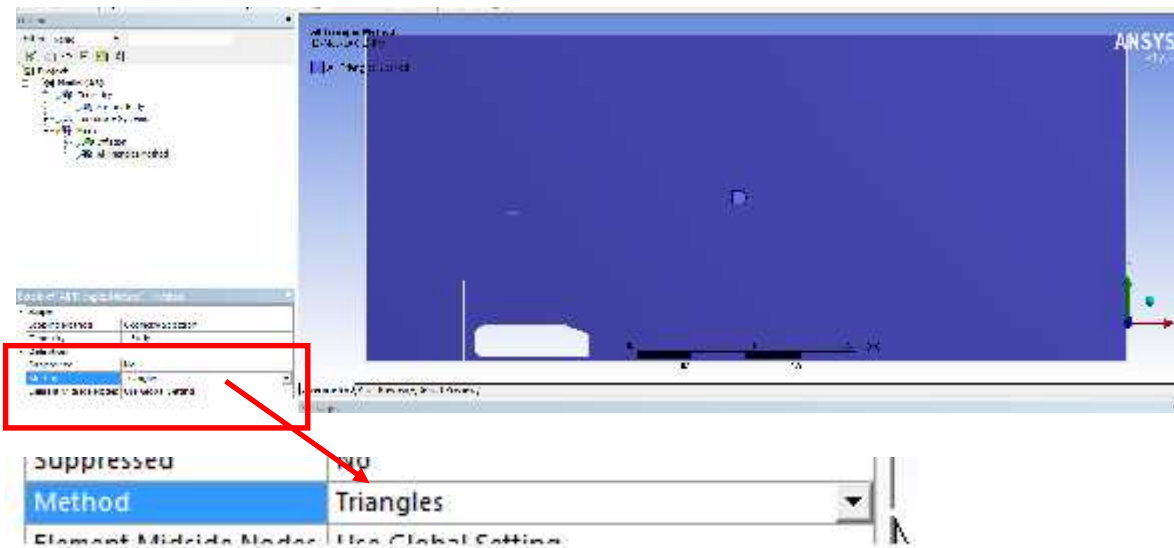


Figure 3.23: Selection of Triangle method for mesh

Now we will define number of grids to be used. In this article we have defined number of divisions so that we can easily divide each portion of car. By using hit and trial method, certain values comes up in order to have precise mesh. So, the values of each portion of body is shown in Table 3.1.

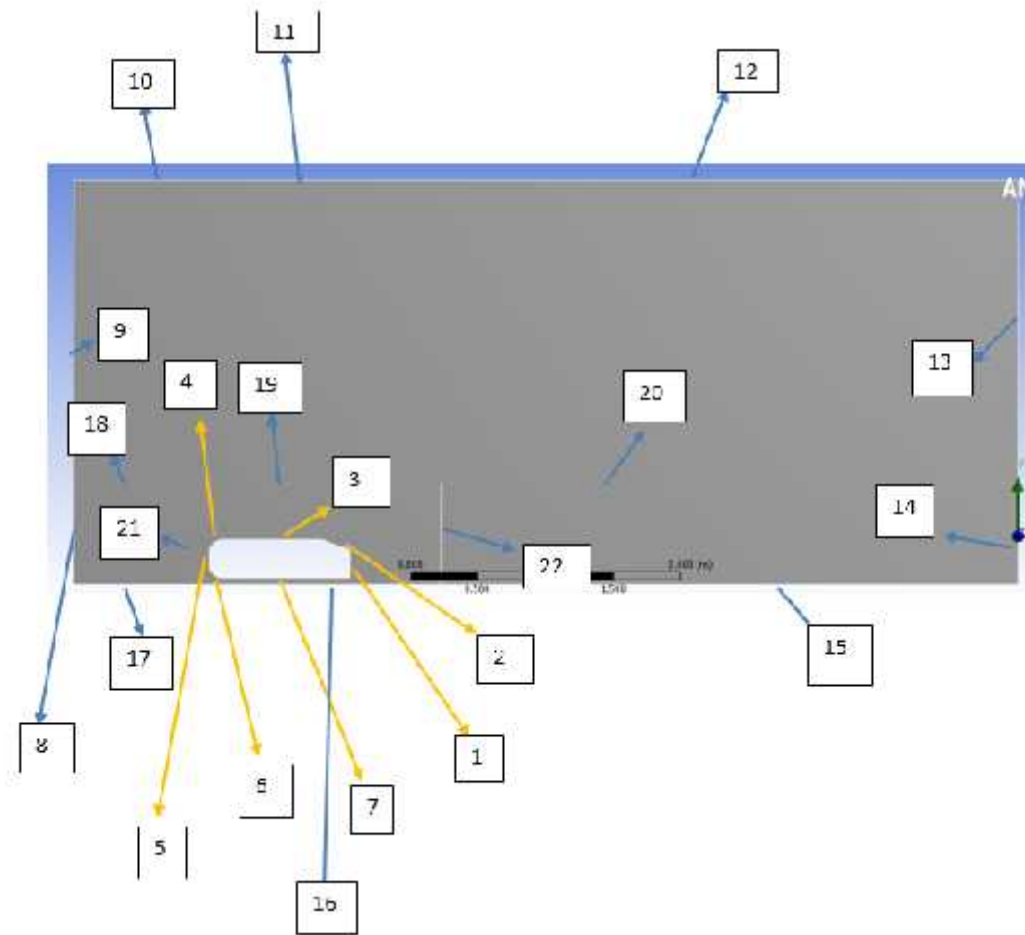


Figure 3.24: Division of body in different parts

Table 3.1: Description of divisions for Meshing

Ref. No.	Number of Divisions	Name of Divisions
1	34	Back of body
2	34	Slope of body
3	104	Top of body
4	23	Nose of body
5	13	Nose of body
6	25	Nose of body
7	169	Bottom of body
8	14	Inlet of body
9	26	Inlet of body
10	6	Symmetry of body
11	17	Symmetry of body
12	26	Symmetry of body
13	11	Outlet of body
14	4	Outlet of body
15	40	Road of body
16	195	Road of body
17	26	Road of body
18	20	Upper portion of body
19	74	Upper portion of body
20	47	Upper portion of body
21	42	Left portion of body
22	24	Right portion of body

After this we will click on “Generate Mesh” and following results we will get from mesh

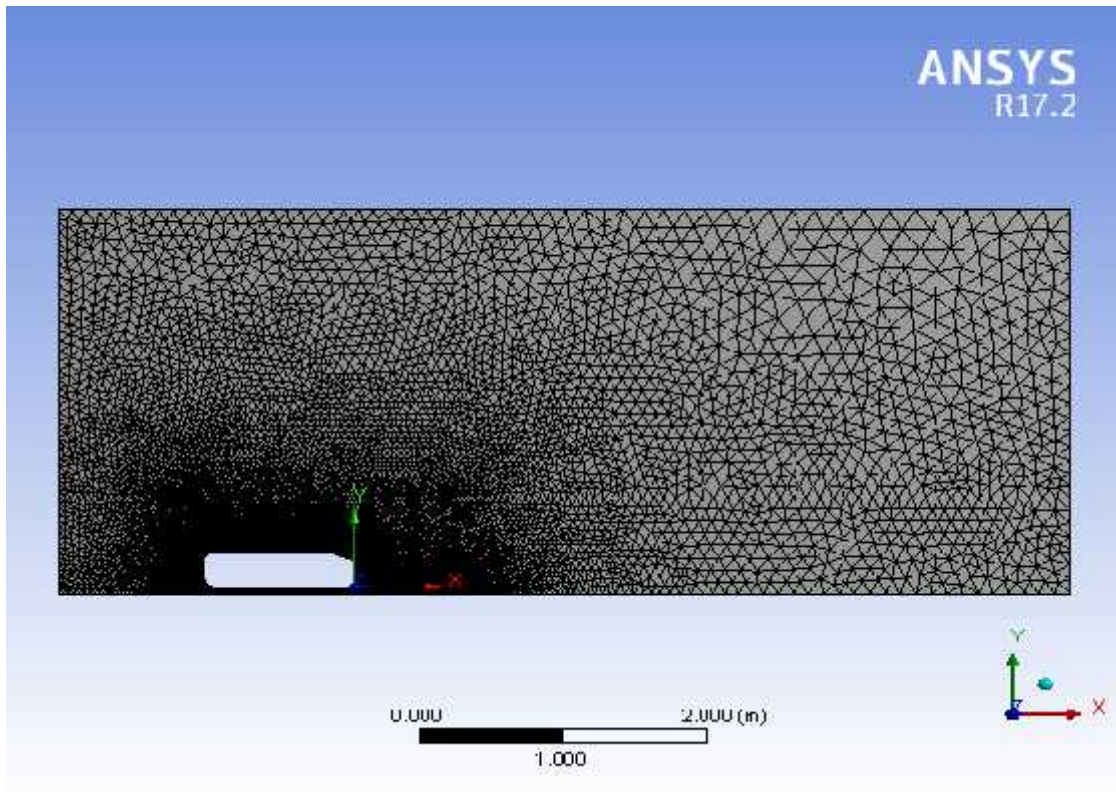


Figure 3.25: Final Mesh

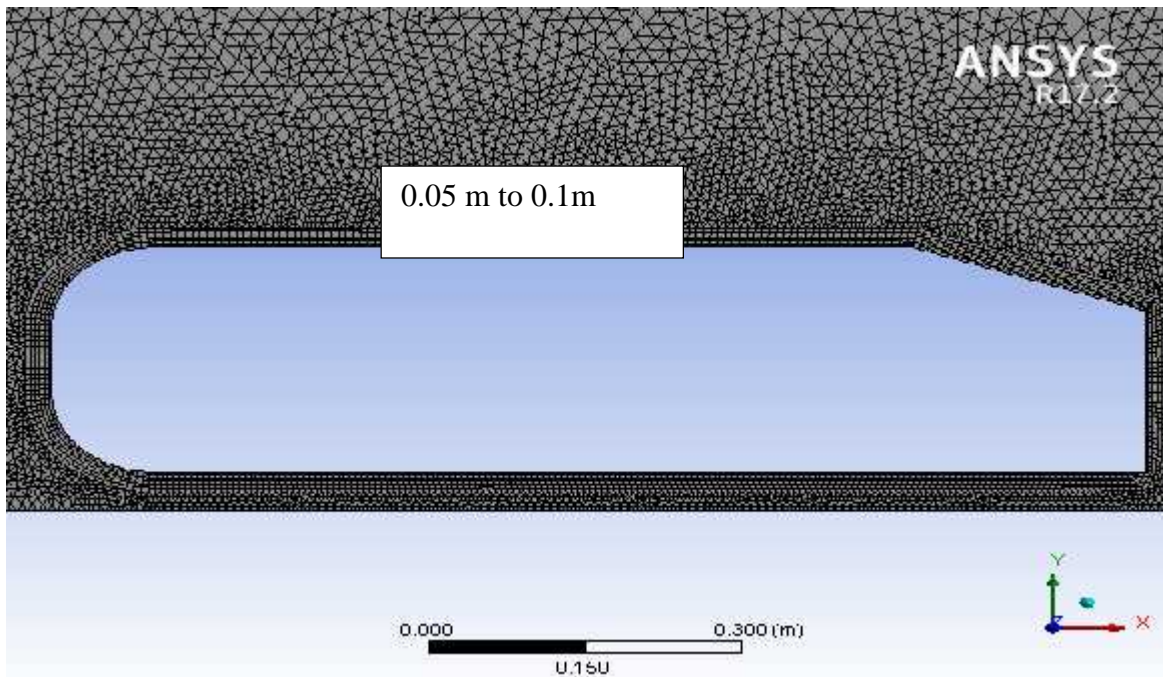


Figure 3.26: Final Mesh zoom-in view

3.2.4 Grid Size

The grid size depends on the nodes and number of elements. The grid size that is found in this study is 0.1m x 0.1m at the edge and starting from 0.05m x 0.05m at the boundary of the body that is obtained after getting mesh that was shown in Figure 3.26

3.2.5 Number of Grid size

Total number of grid depends upon total number of elements and nodes that are used in the mesh setup. Below figure shows the numbers that are required

Node represents the grid point and elements indicates number of grids present as shown in Figure 3.27.

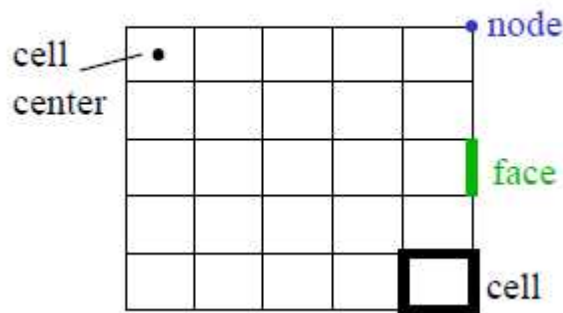


Figure 3.27: Nodes and elements demonstration

+ Advanced	
- Statistics	
<input type="checkbox"/> Nodes	13592
<input type="checkbox"/> Elements	25500
Mesh Metric	None

Figure 3.28: Nodes and elements value came from ANSYS

After generating mesh, we have to give names to each corner so that we can have solution as per respective requirements. For this we will use “Create Named Selection” to name each corner.

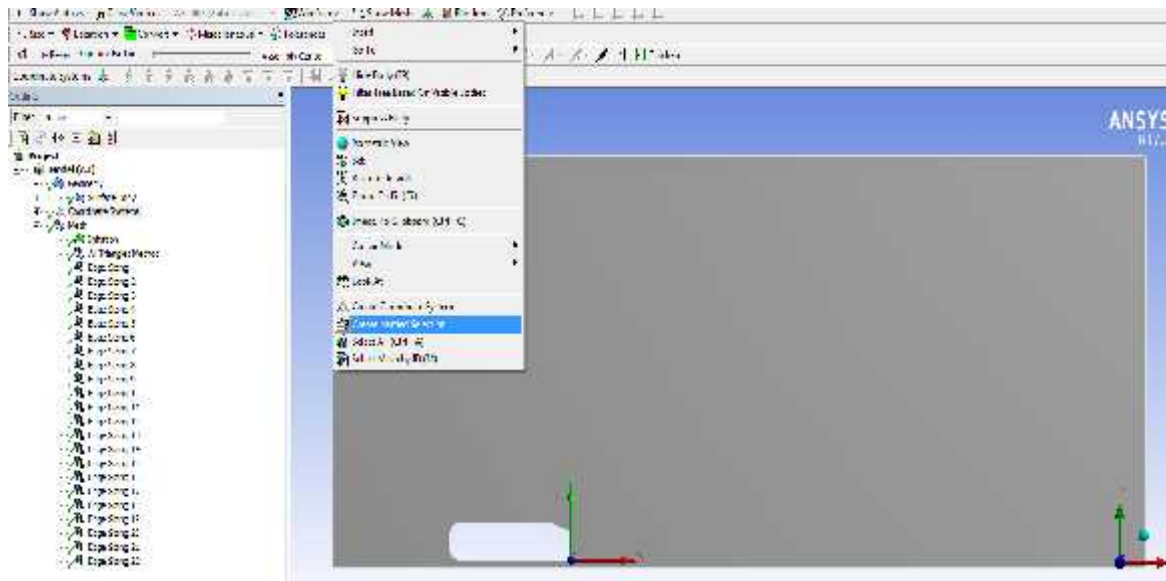


Figure 3.29: Using Named Selection command

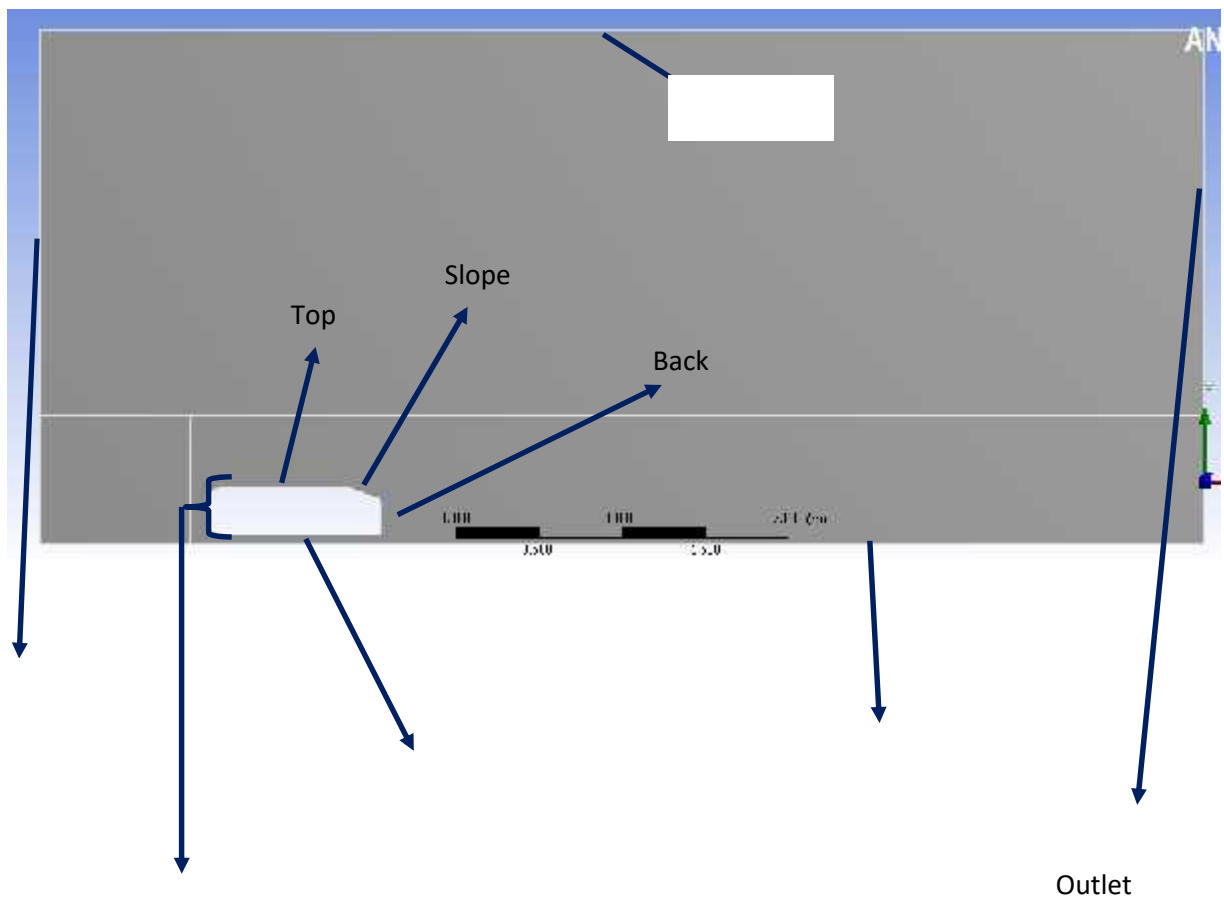


Figure 3.30: Name of different portions of Ahmed body

3.3 Setup

Now after completing meshing, we will start setup in which we have to insert boundary conditions and all the required data that needs to be inserted in the model.

First we will have this window open. For simulation, we have taken 2D so we don't have to change anything.

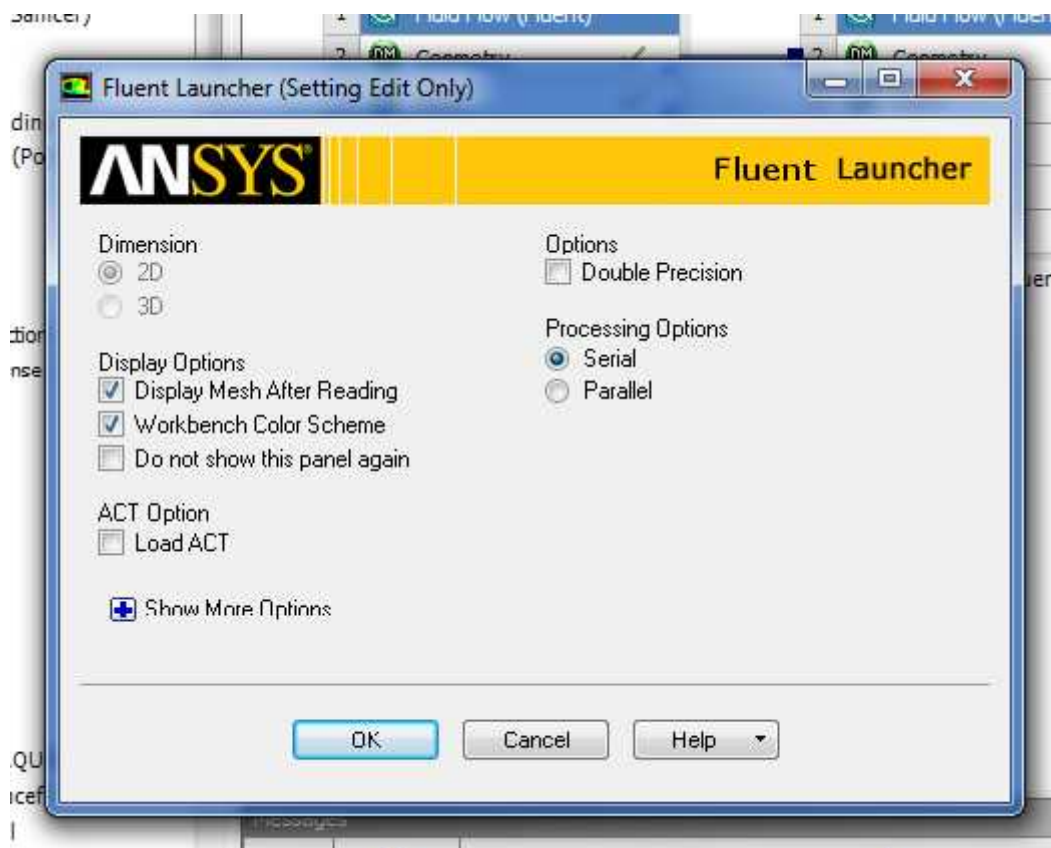


Figure 3.31: Fluent launcher

Then we will describe time to be transient shown above in Figure 3.31. The reason why we have not taken time to be steady because steady time neglects advanced order terms with respect to time but whereas transient time involves all terms. Transient model takes time in order to converge the results but is efficient as compared to steady time simulation. The below picture shows how time has been chosen.

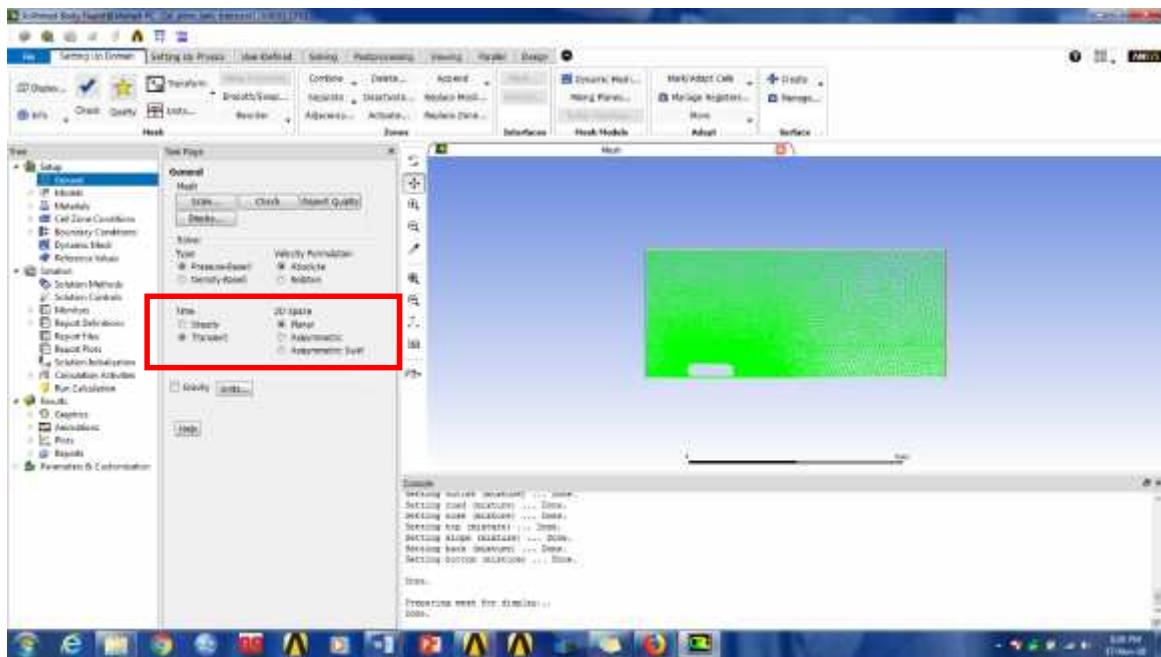


Figure 3.32: Selection of transient time

After that we will define the model in which we will select the near wall treatment to be “Non-equilibrium wall force”. The reason why we have selected this option because non-equilibrium wall functions are generally specified for complex flows in which the pressure gradient is changing drastically. It is often used to calculate the wall shear coefficient and Nusselt or Stanton number

This method is applicable to the below viscous models but in this case, we will use standard k-epsilon method

The step is mentioned below in the Figure 3.33.

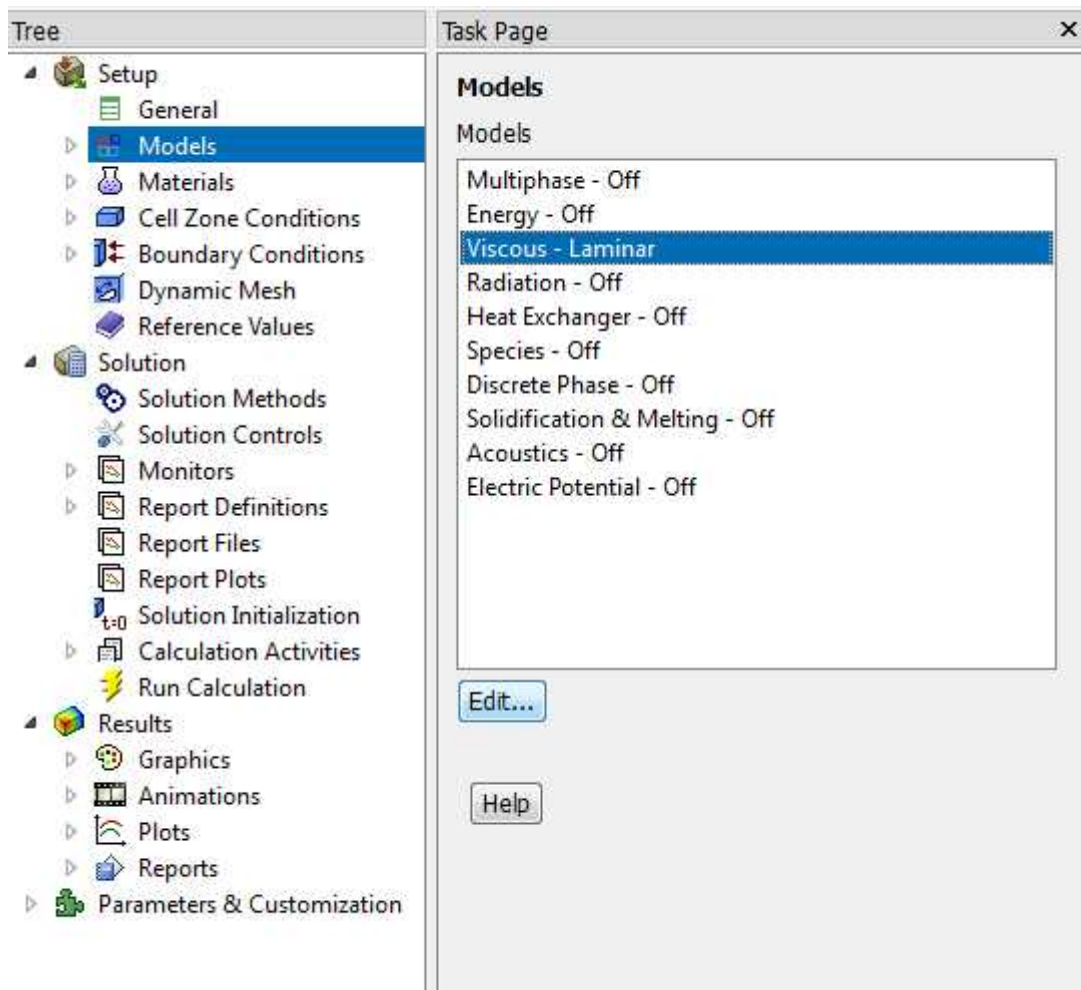


Figure 3.33: Selection of viscous model

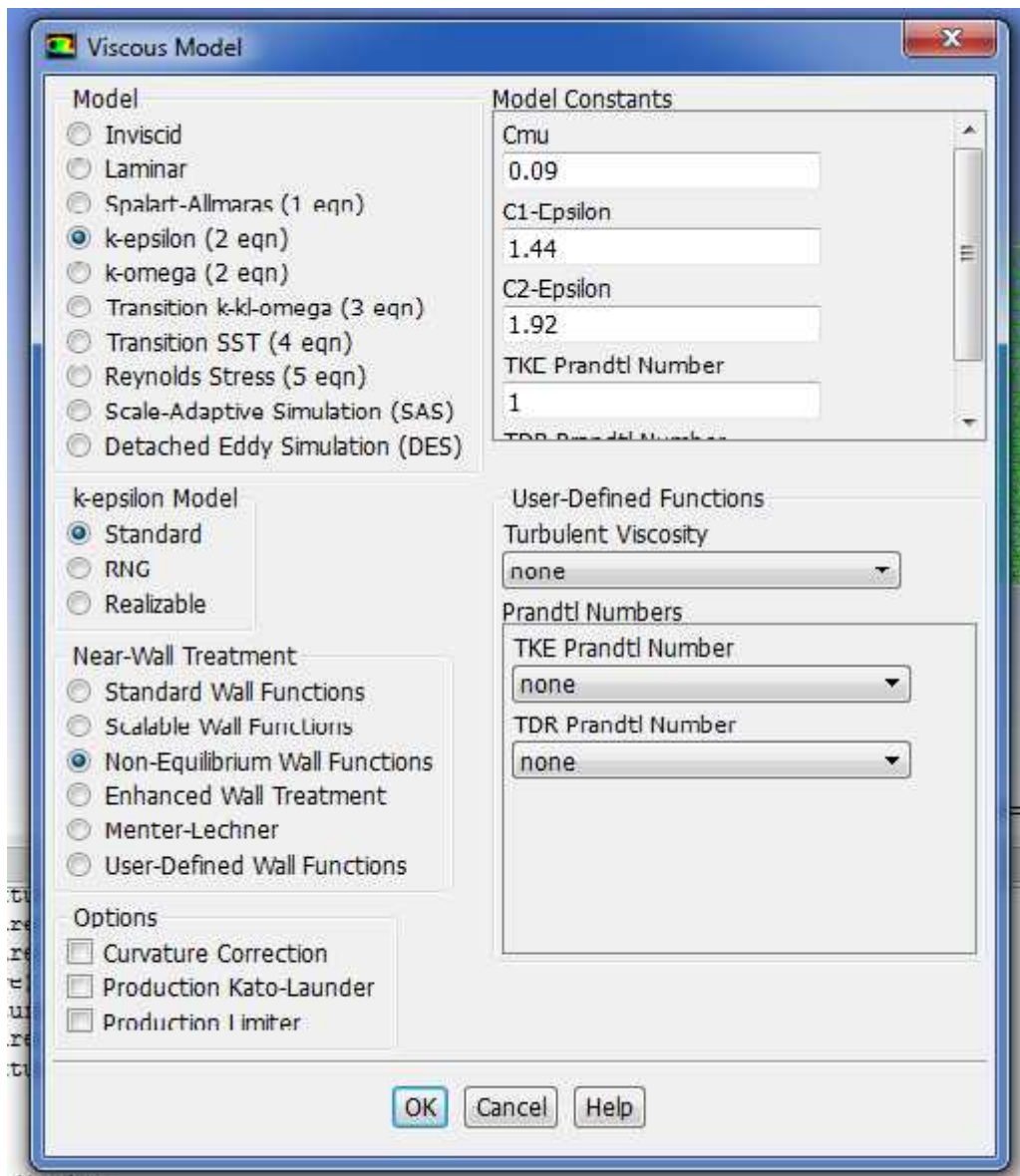


Figure 3.34: Display of values taken for k-epsilon model

After this, we will define the boundary conditions at the inlet and outlet. So at inlet, we will define the inlet velocity to be 40 m/s as shown in Figure 3.35.

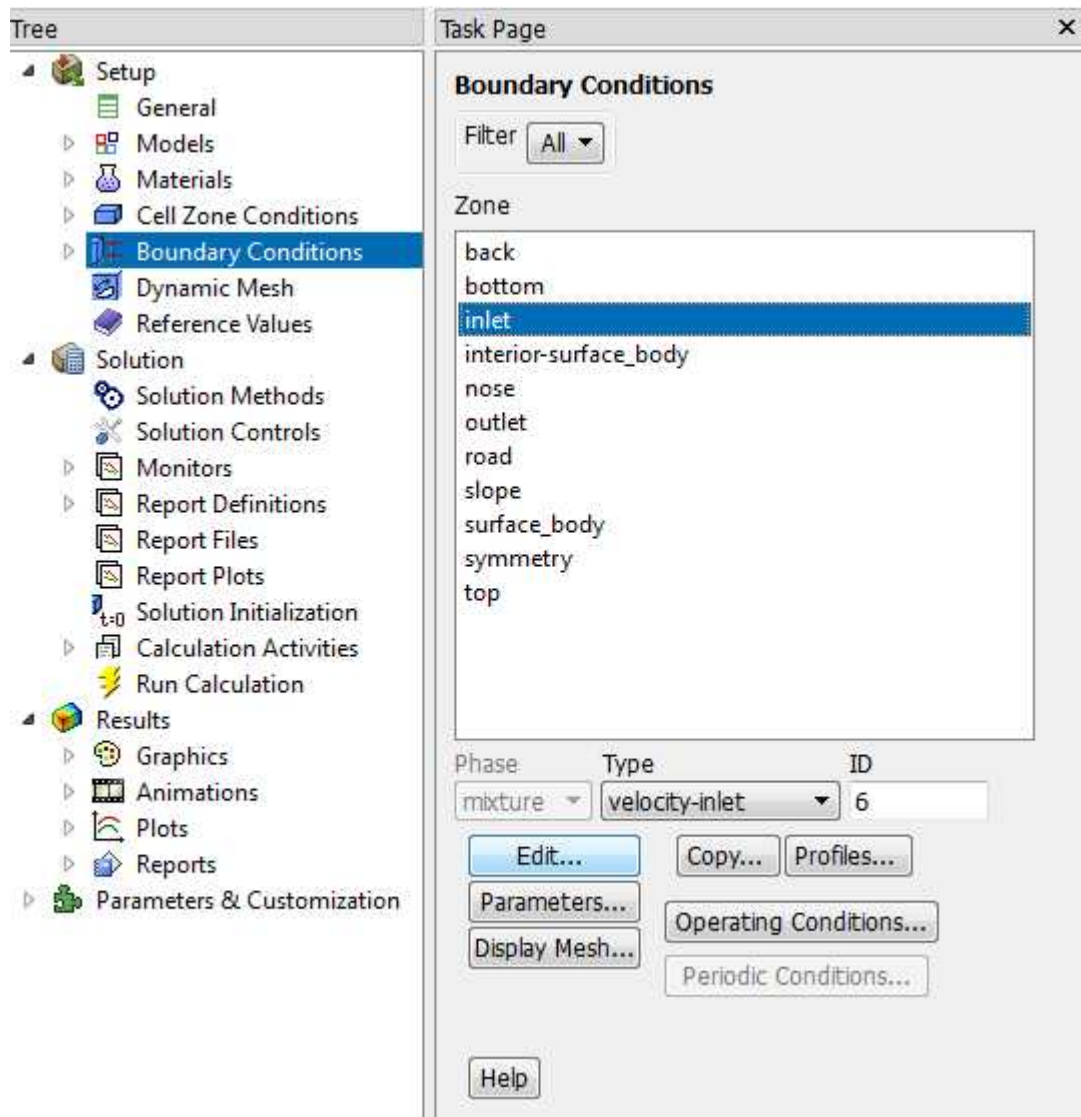


Figure 3.35: Selecting inlet conditions

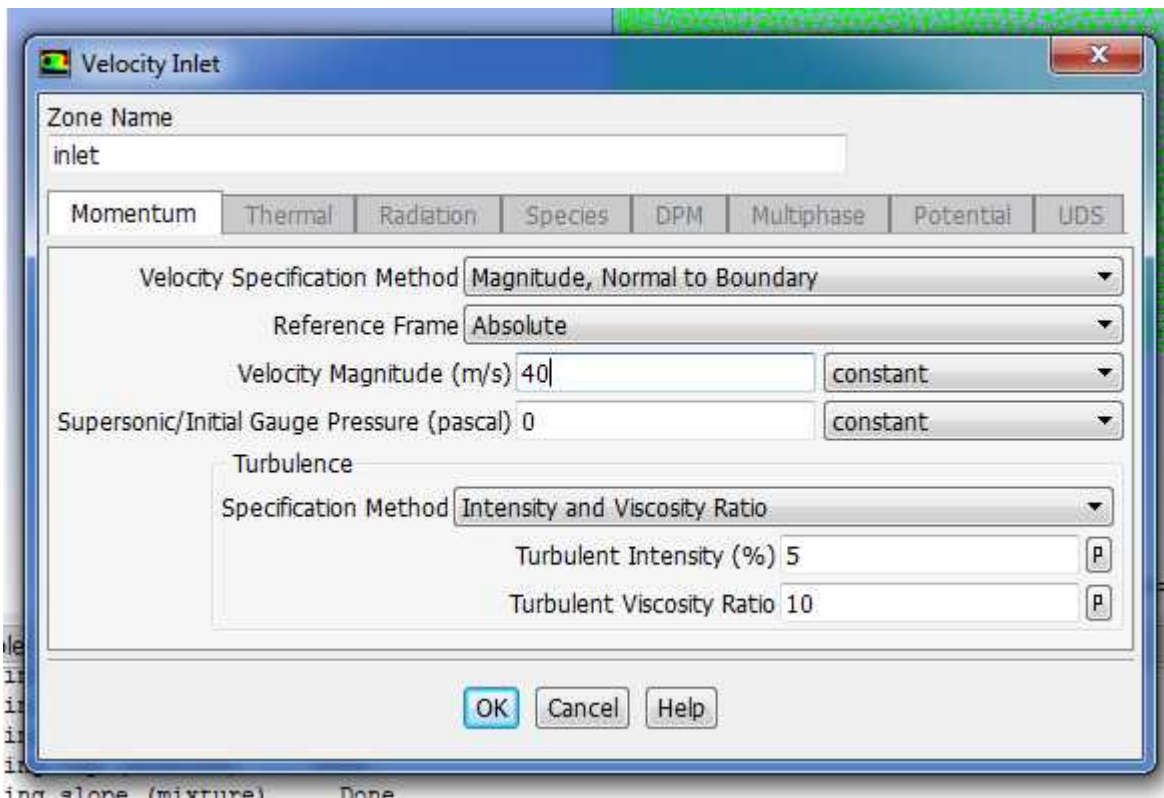


Figure 3.36: Selecting velocity value

Now, we have to define the area, density, and velocity by using command of “Reference Values”.

The values are mentioned in below Figure 3.37.

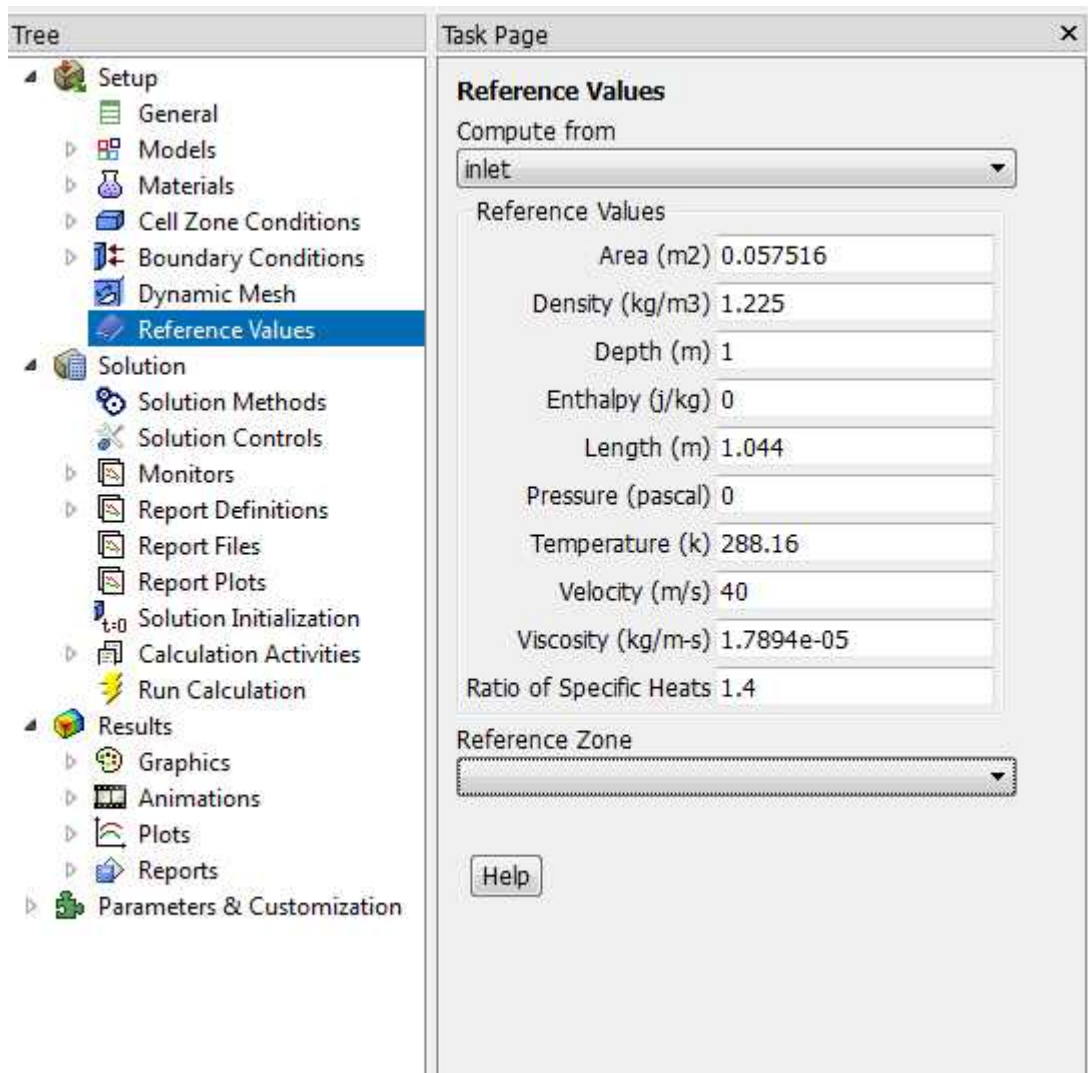


Figure 3.37: Selecting area and length

After this, we will describe the “Solution Manual” in which we will describe Gradient, Scheme and Pressure. So first, we will describe method of PISO, PRESTO and Green-Gauss Cell based.

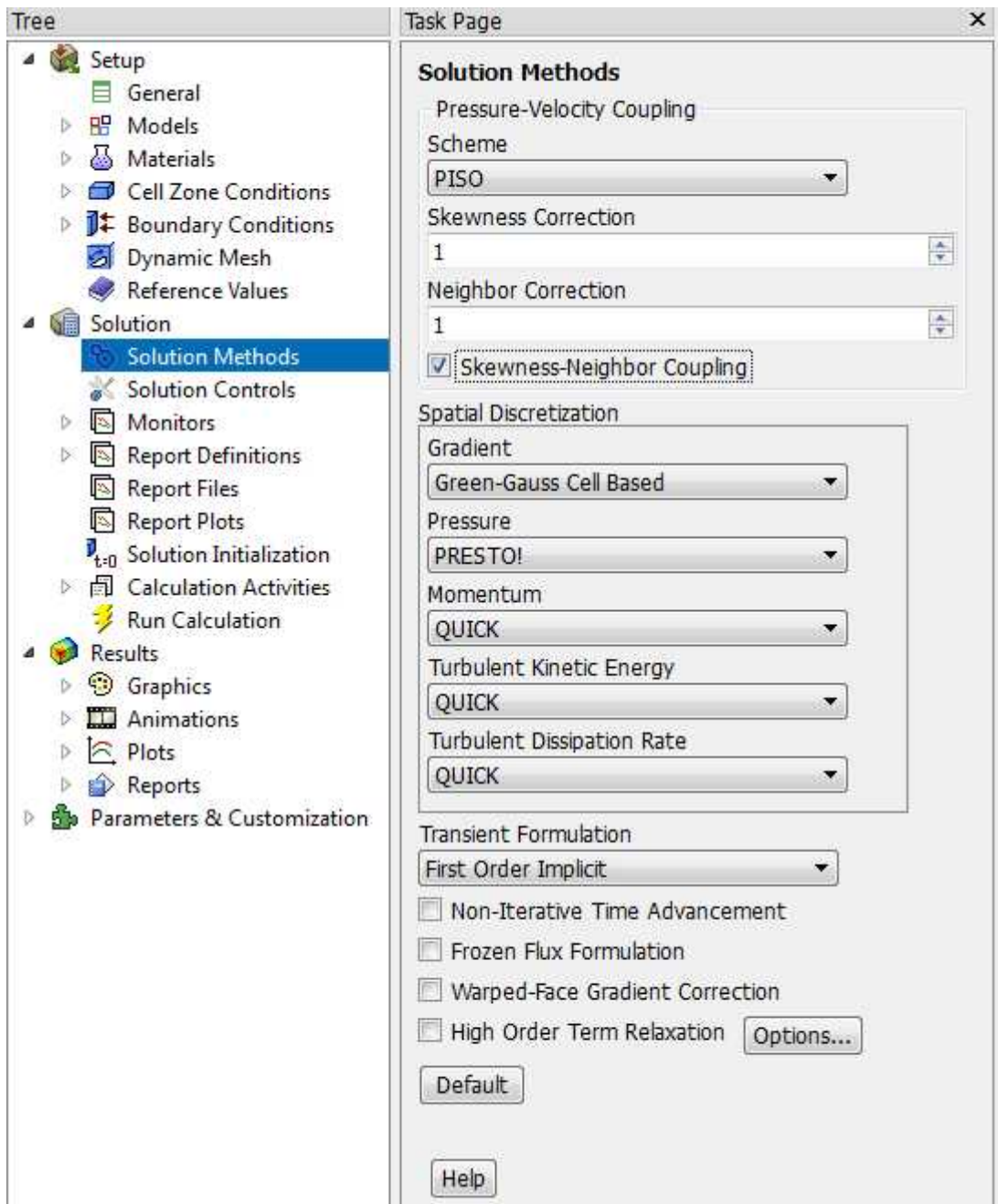


Figure 3.38: Selection of Solution Method

3.3.1 Scheme

Scheme method consists of different methods that includes:

-) PISO
-) SIMPLE
-) SIMPLEC
-) Coupled

PISO is useful for the unsteady flow and also for large skewness number. SIMPLE method is always the default option in the ANSYS. SIMPLEC enables to have solution at a quick rate and Coupled method is almost same as PISO.

In our case, we have used PISO because it helps in calculating Navier-Stokes equations.

3.3.2 Spatial Discretization

It is divided into five regions namely Gradient, Pressure, Momentum, Turbulent Kinetic Energy and Turbulent dissipation rate which is further discussed below

➤ *Gradient*

It consists of four methods:

-) Least Square cell based
-) Green Gauss cell based
-) Green Gauss node based

Least square method uses for polyhedral meshes. Green gauss node based is utilized to decrease false diffusion usually used for tri meshes and Green gauss cell based method helps finding value between two cells by approximating the values.

In this case, we will use Green gauss cell based method.

➤ *Pressure*

This approach comprises of certain procedure that includes

-) Standard
-) PRESTO
-) Linear
-) Second-Order
-) Body force weighted

Standard method is used for big surface pressure gradients close to boundaries. PRESTO method is utilized for high swirling flows that includes large pressure gradients whereas linear method is used due to unphysical approach. Second order use when flow is compressible and Body force weighted is picked when body force are huge.

In this case, we will use PRESTO method because of large swirl numbers.

➤ *Momentum*

This method also contains some approaches namely

-) First-Order upwind
-) Power law
-) Second-Order upwind
-) Third-Order MUSCL
-) QUICK

First-order method is the simplest method that contains first order accuracy. Power law used normally for $Re < 5$. Second-order upwind is utilized for the flows that are not converged, gives 2nd order accuracy. Third-order MUSCL is used for 3rd order solutions for unstructured meshes and finally QUICK method uses for uniform mesh and also 3rd order accuracy.

We will use QUICK method in order to have an accuracy in results.

Now, after completing all the boundary conditions, we will now access the calculation domain. So, we will define number of time step size to be 1400 and Time step size to 1400 in order to have the solution to be converged displayed in Figure 3.39.

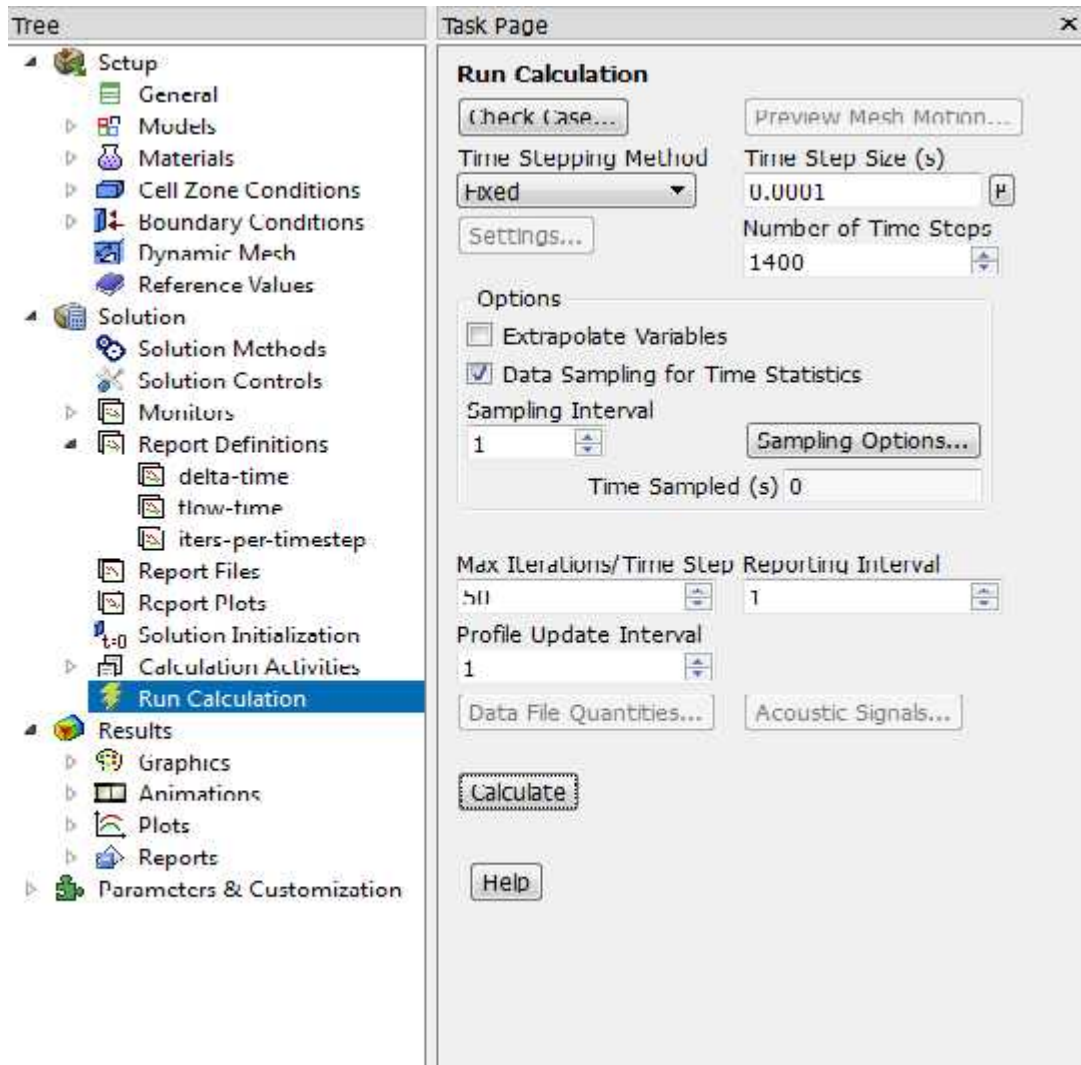


Figure 3.39: Display of Run calculation

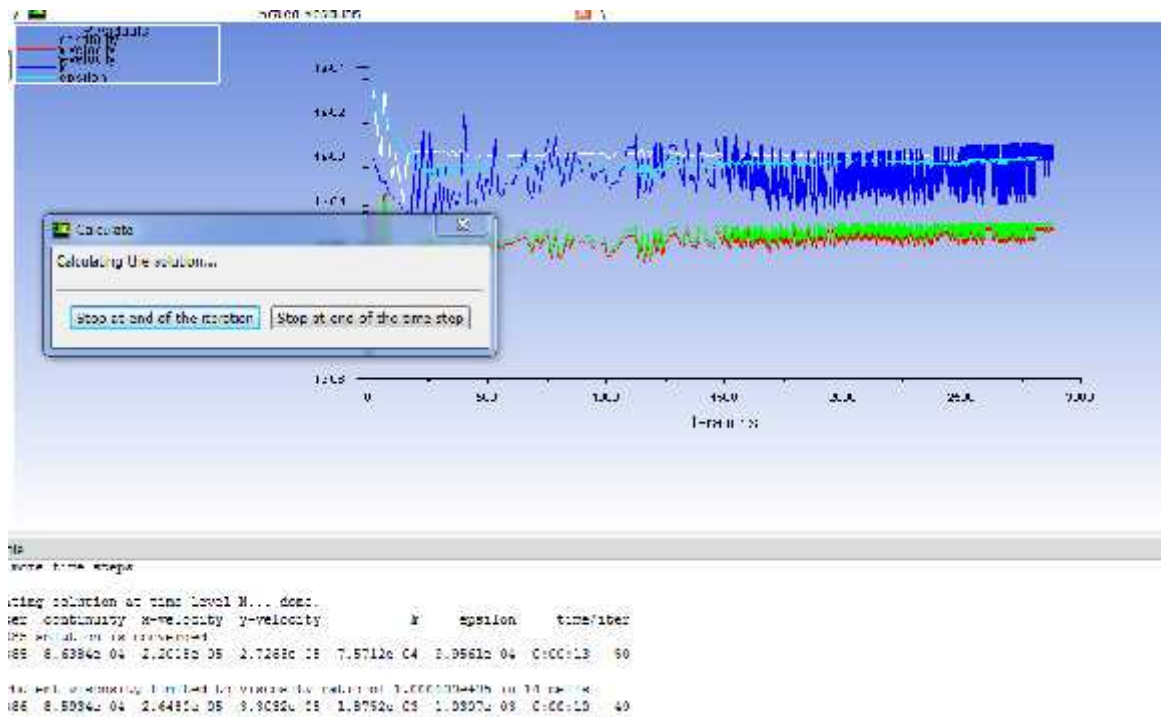


Figure 3.40: Display of number of iterations against time

CHAPTER 4

RESULTS AND DISCUSSIONS

After inserting boundary conditions, we will look into the results in order to see velocity and pressure contours and also drag force and then compare with yaw angles consisting of 0° , 20° , 40° , 60° and 80° . So, first we will look into drag force as shown in below Figure 4.1

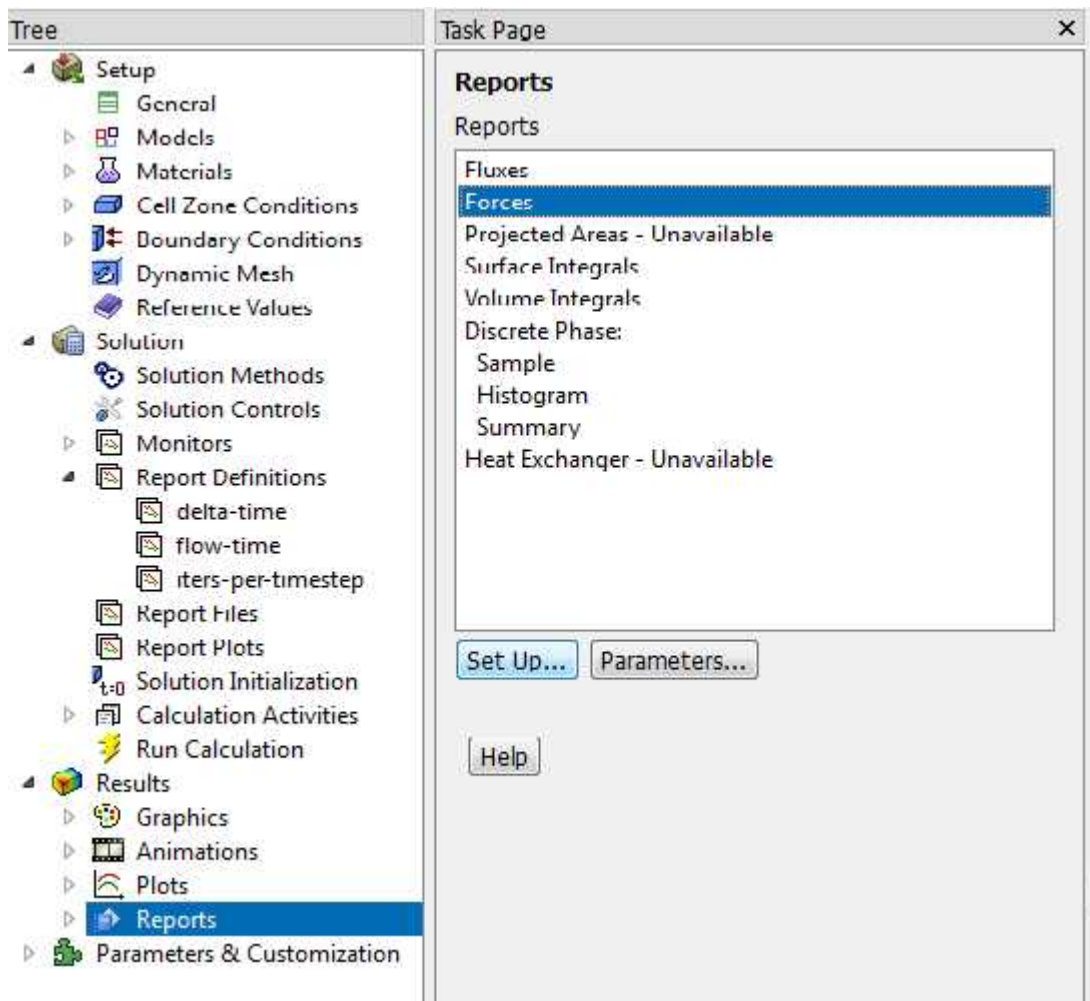


Figure 4.1: Display of reports after running the results

So, C_D is calculated to be 0.67 as per the solution.

Now, we will calculate pressure and velocity contour for 20° yaw angle as shown in Figure 4.2

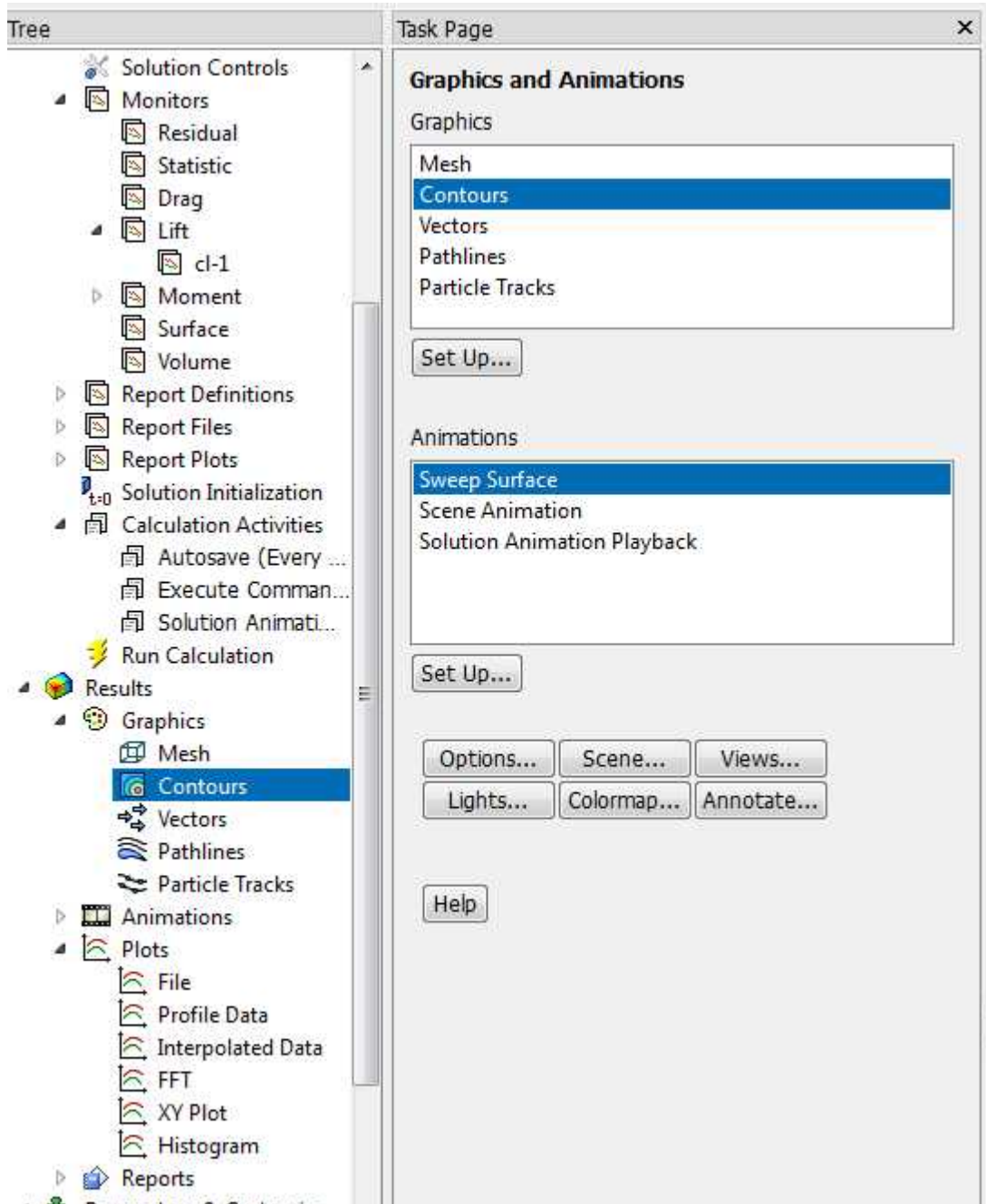


Figure 4.2: Contours for pressure and velocity profiles

Force	X	Y	Z	Value	Value	Value
total	-0.4972221	2.0036611	-0.0030674	-0.37048077	0.001672114	-0.000174266
mom	0	21.871323	21.871323	0	0.038772880	0.038772880
jet	0.2126760	33.430030	16.06048	0.21052650	0.059222107	0.2773700

Figure 4.3: Display of drag force after simulation

4.1 Pressure and Velocity Profiles

4.1.1 20° Angle

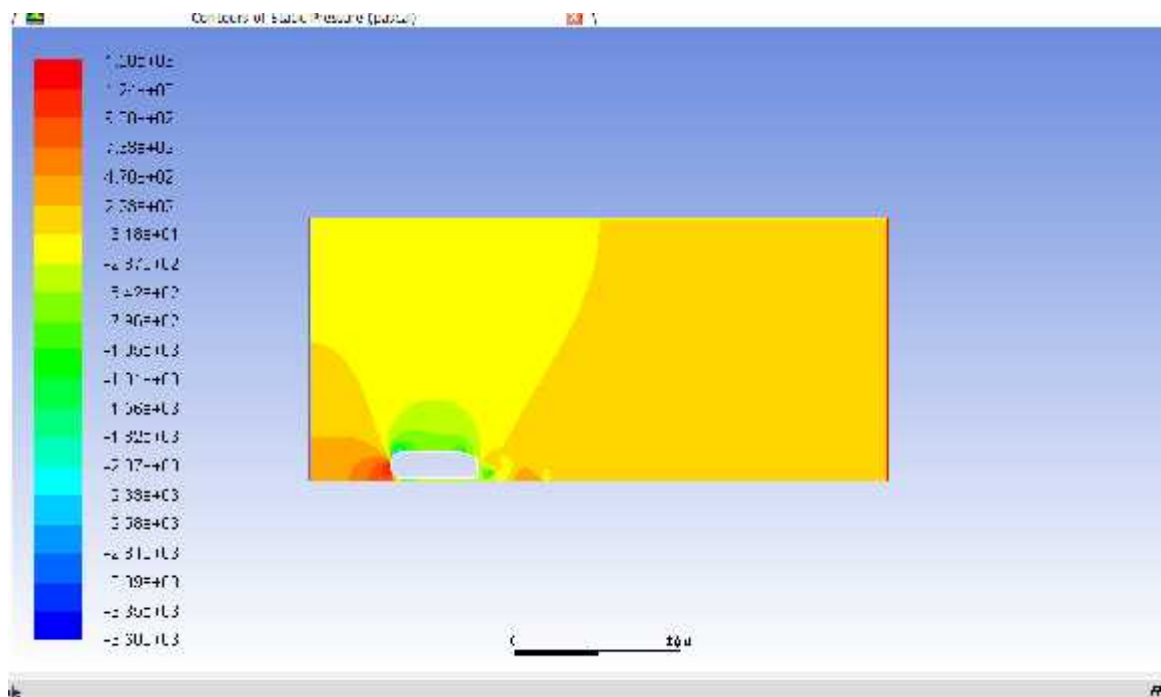


Figure 4.4: Pressure profile for 20° angle

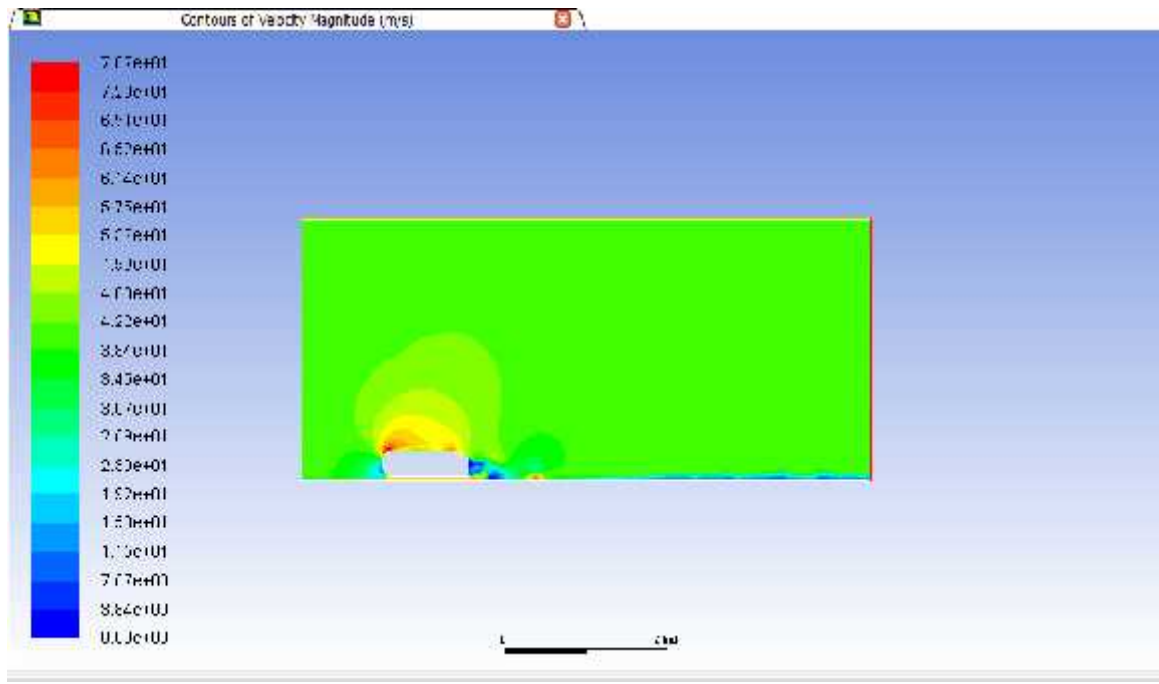


Figure 4.5: Velocity profile for 20° angle

Now, we will compare velocity and pressure contours for different angles that is 0°, 20°, 40°, 60°, 80°. So first we will describe contours of 40°

4.1.2 0° Angle

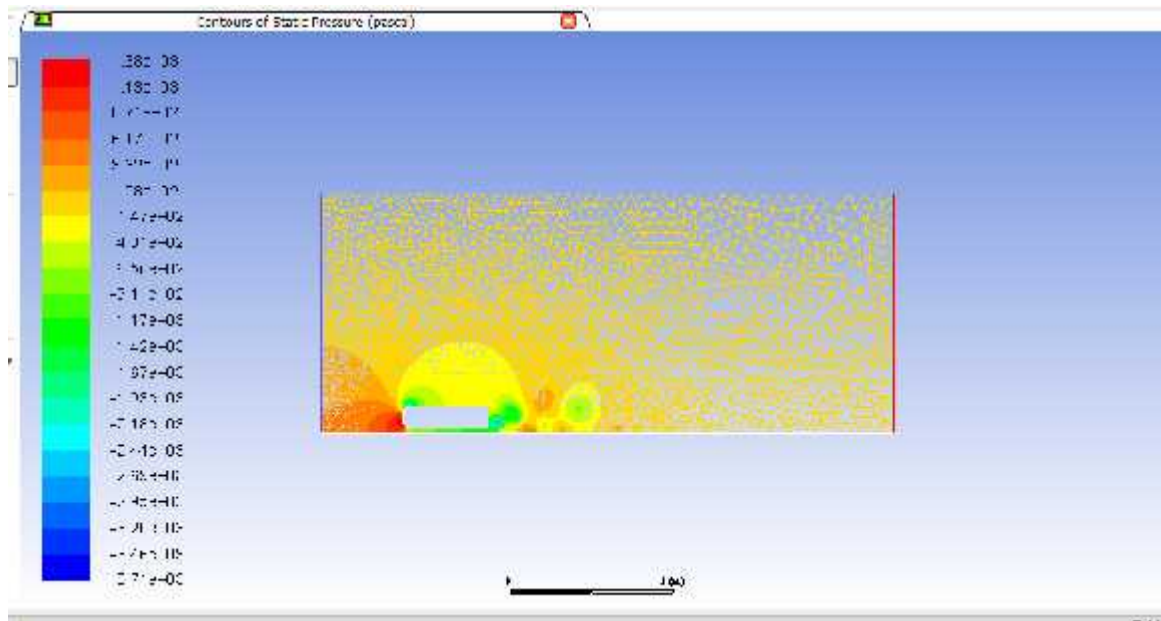


Figure 4.6: Pressure profile for 0°angle

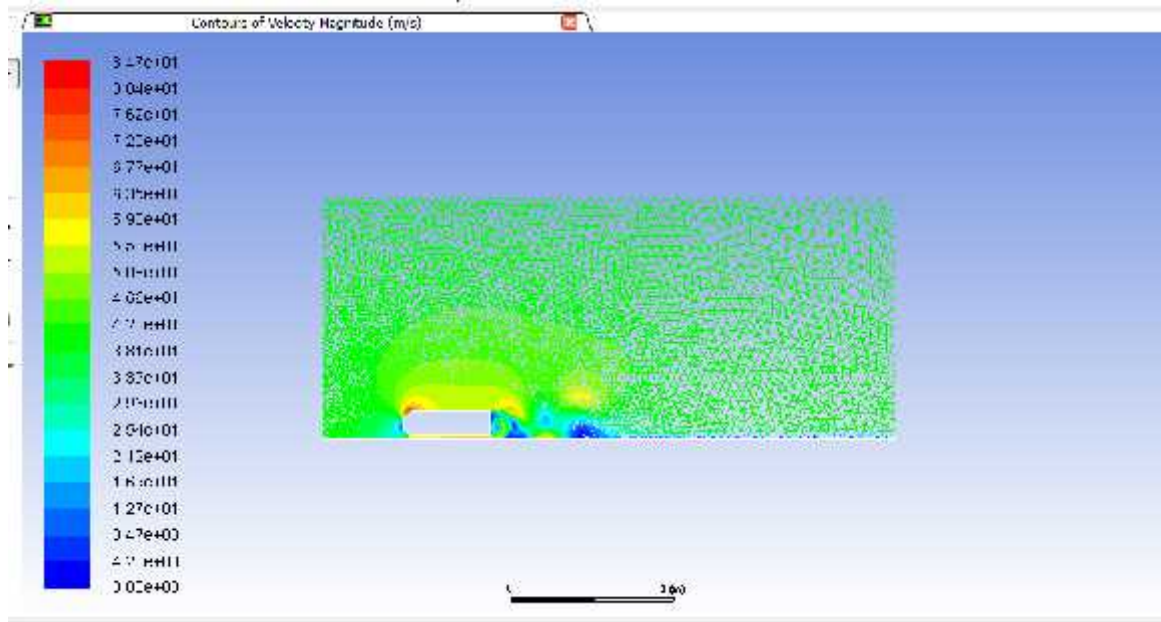


Figure 4.7: Velocity profile for 0°angle

4.1.3 40° Angle

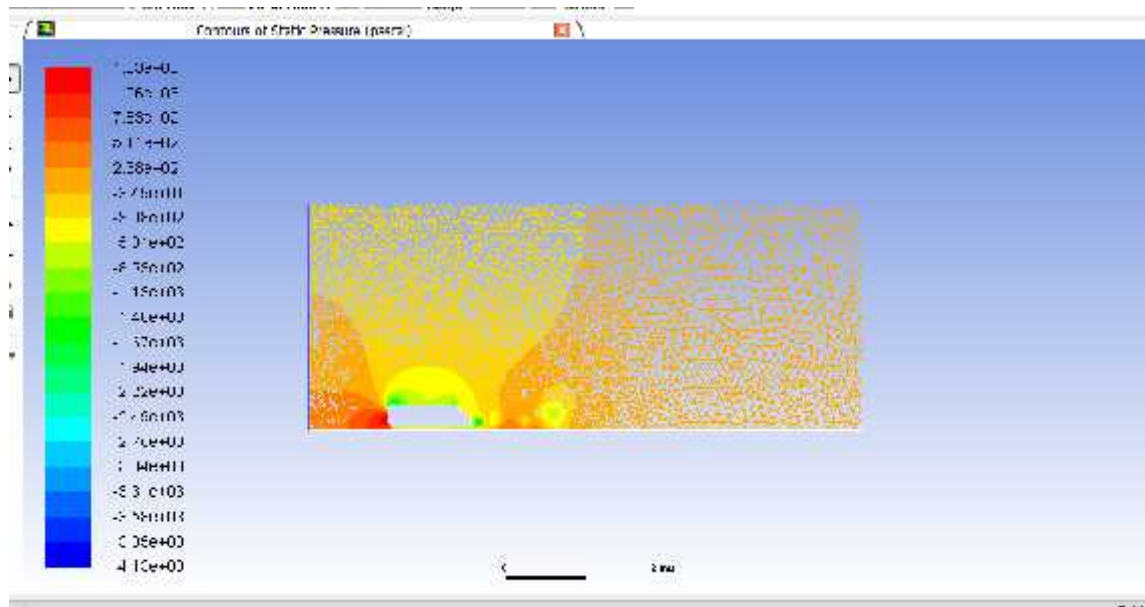


Figure 4.8: Pressure profile for 40° angle

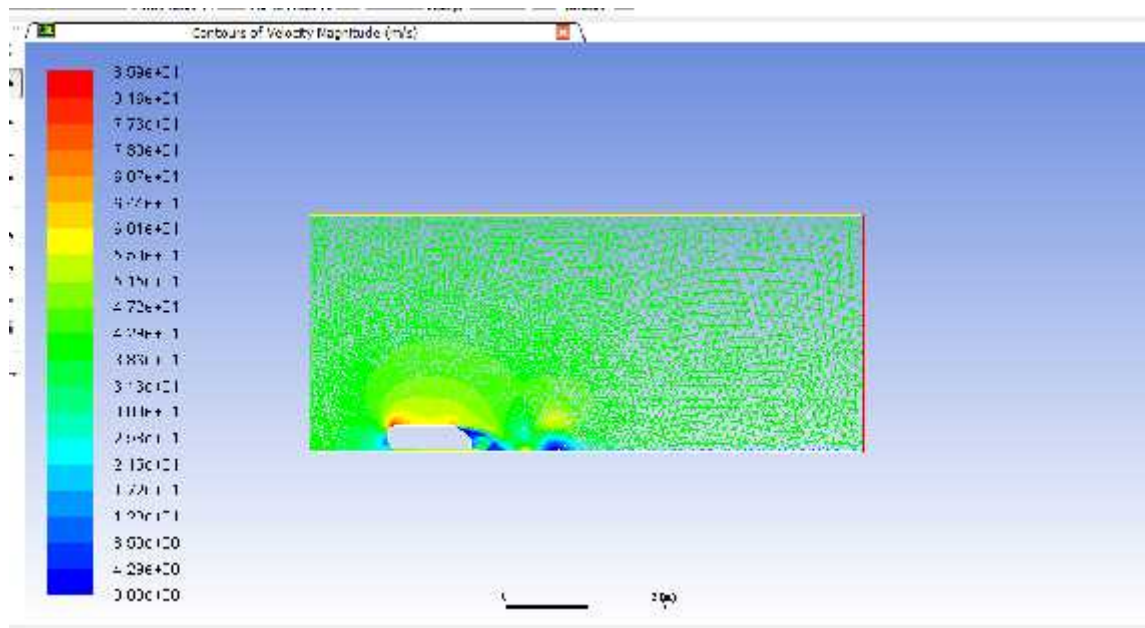


Figure 4.9: Velocity profile for 40° angle

4.1.4 60° Angle

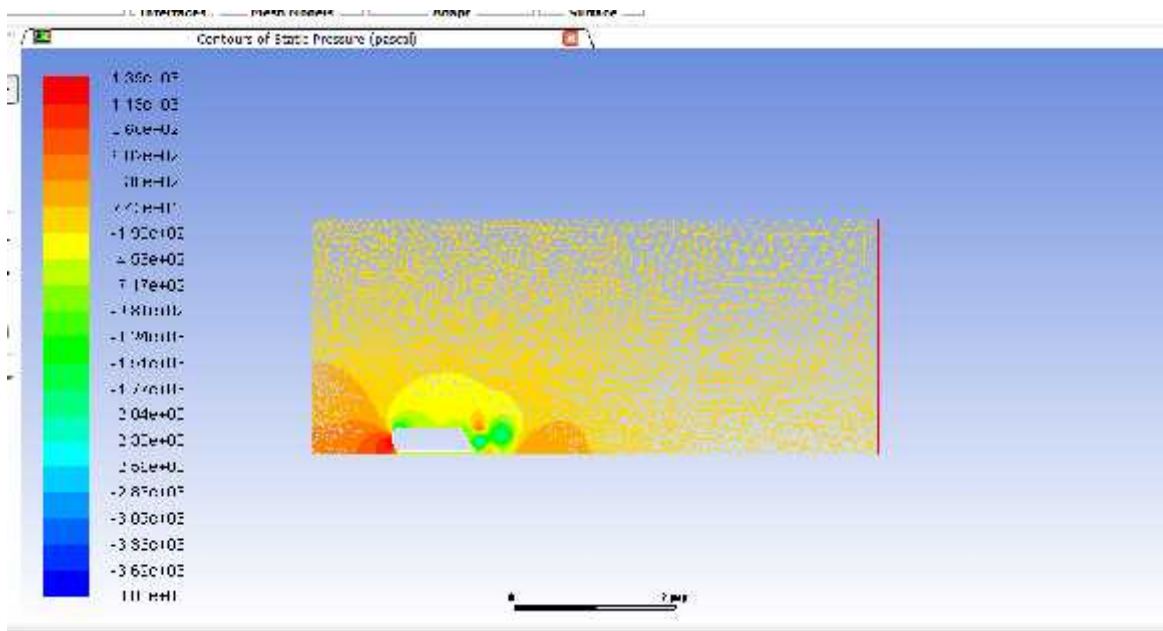


Figure 4.10: Pressure profile for 60° angle

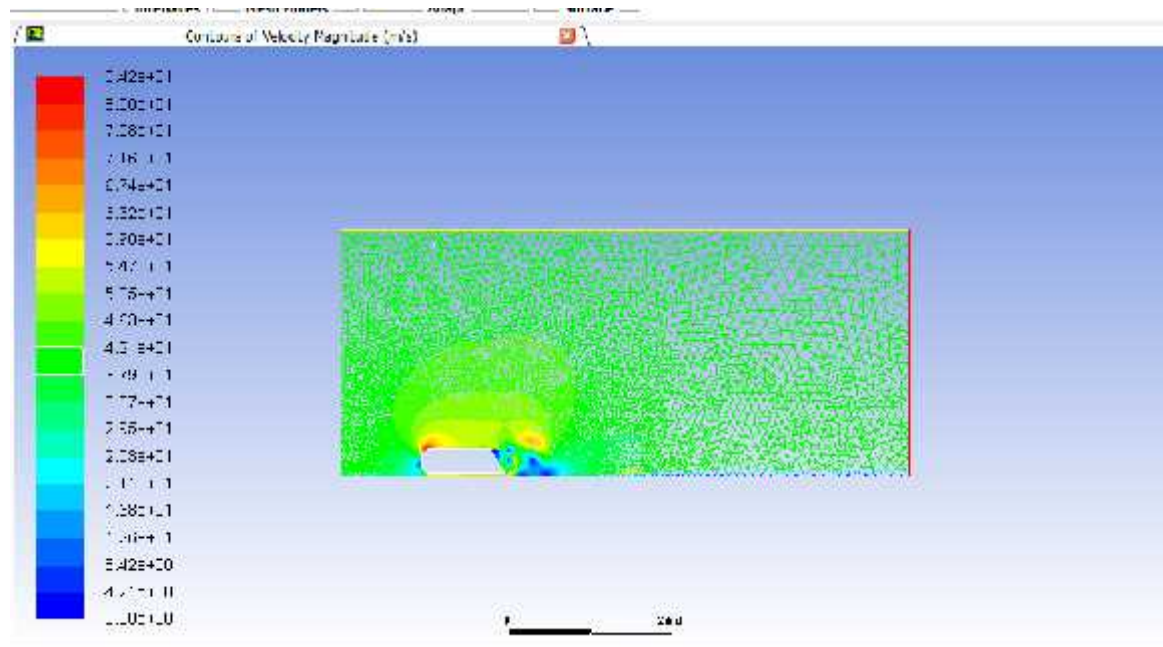


Figure 4.11: Velocity profile for 60° angle

4.1.5 80° Angle

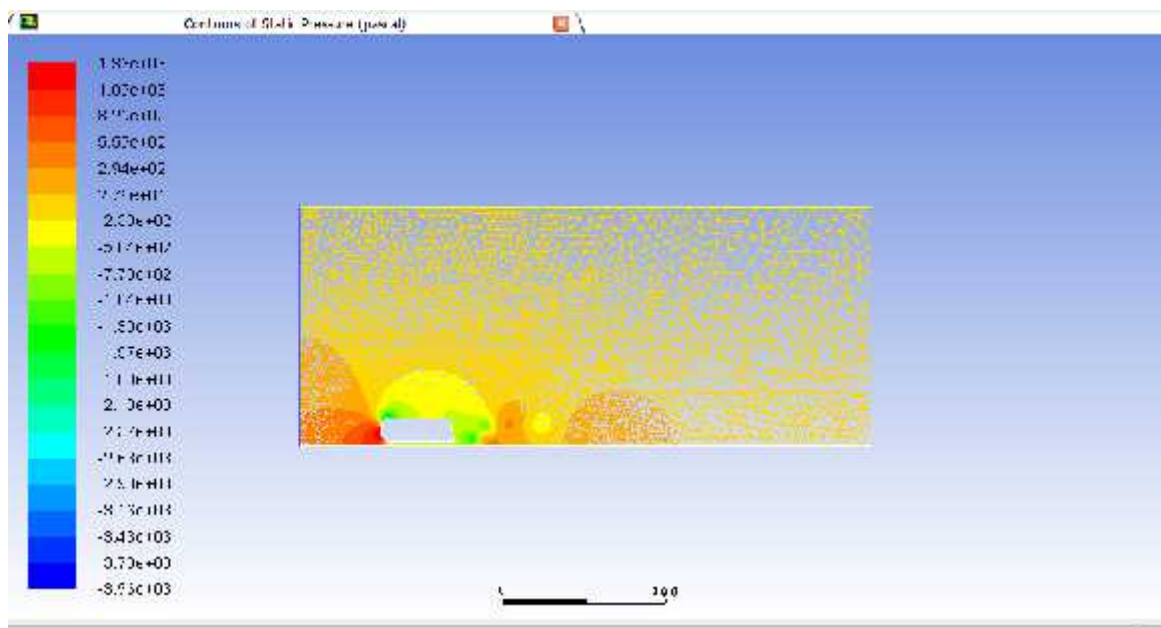


Figure 4.12: Pressure profile for 80° angle

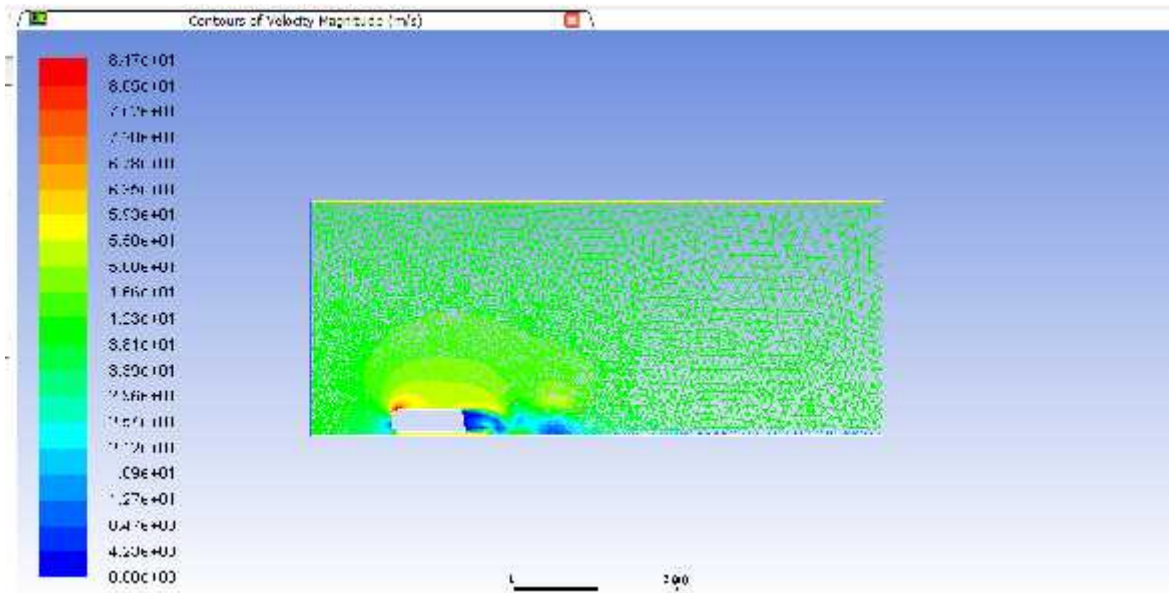


Figure 4.13: Velocity profile for 80° angle

The velocity and pressure profile indicates that the flow is expanded as we increase the yaw angles and the flow is not converged, it shattered in different region across the body. It indicates that it is optimal to use yaw angles from 0° to 40° for optimal condition of Ahmed body

4.2 Drag Coefficient

Now we will look into the drag coefficients for different angles in order to analyze results. For this, we will draw Table 4.1 that demonstrates different drag coefficients for different angles.

Table 4.1: Drag Coefficient for different Yaw Angles

Yaw Angles	C_D (F.J. Bello-Millan 2016)	C_D (Present Values)
0°	0.4	0.24
20°	0.8	0.277
40°	1.7	1.77
60°	2.25	4.07
80°	2.3	3.62

The table shows that the drag co-efficient that have obtained after CFD analysis indicates that the best yaw angles that can be used for having best performance is between 0° to 40° and after that the drag co-efficient values diverge a lot from the experimental setup indicates that it is not feasible to use the angles larger than 40°.

After analyzing the data, it is concluded that the current result is 33.91% accurate as compared to the experimental data indicating that the use of CFD enhance the accuracy.

Now, we will demonstrate the results through graphs. First, the graph shows relationship of yaw angles and drag coefficient that has the values that was previously used in the experimental setup by F.J. Bello-Millan et al., (2016) and then we will take readings from the present readings and then compared both with each other.

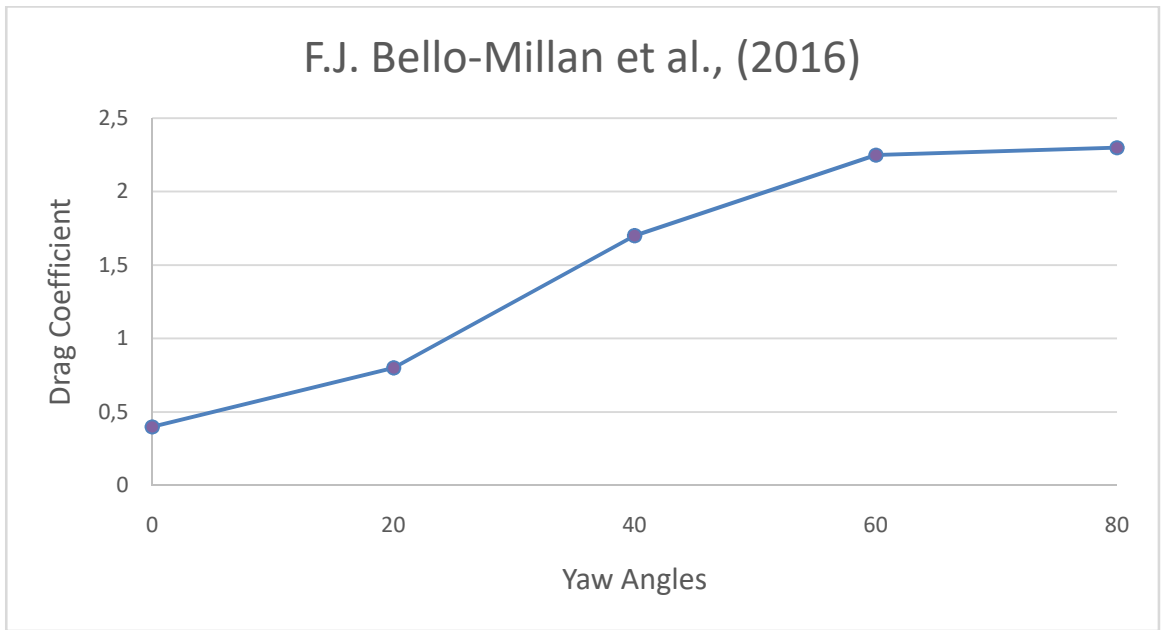


Figure 4.14: Graph of experimental results of drag coefficient against different yaw angles

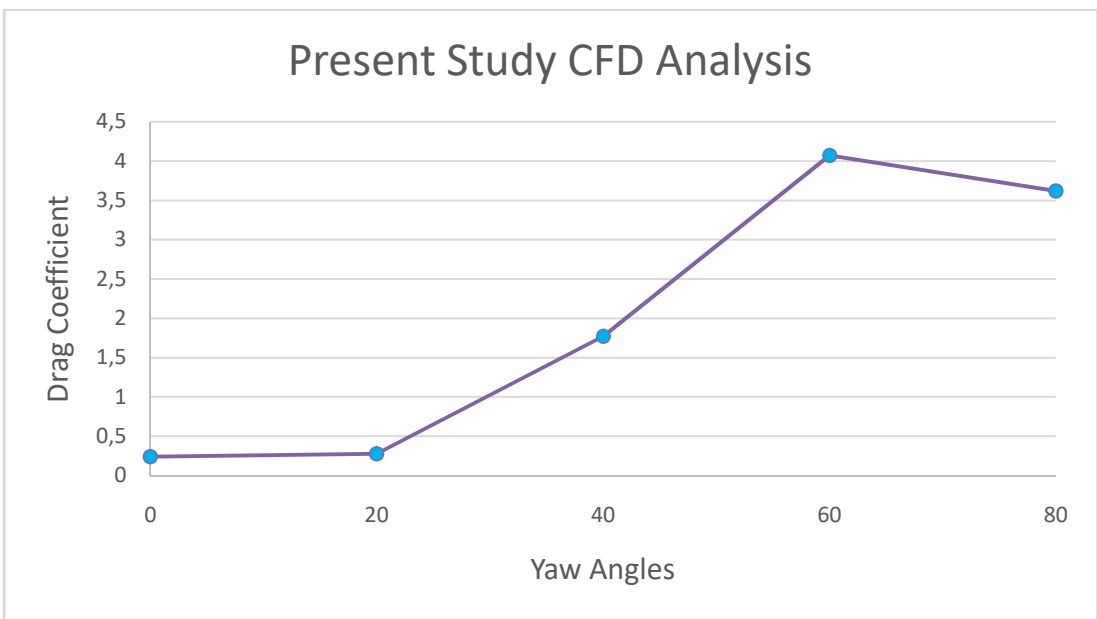


Figure 4.15: Graph of present findings of drag coefficient against different yaw angles

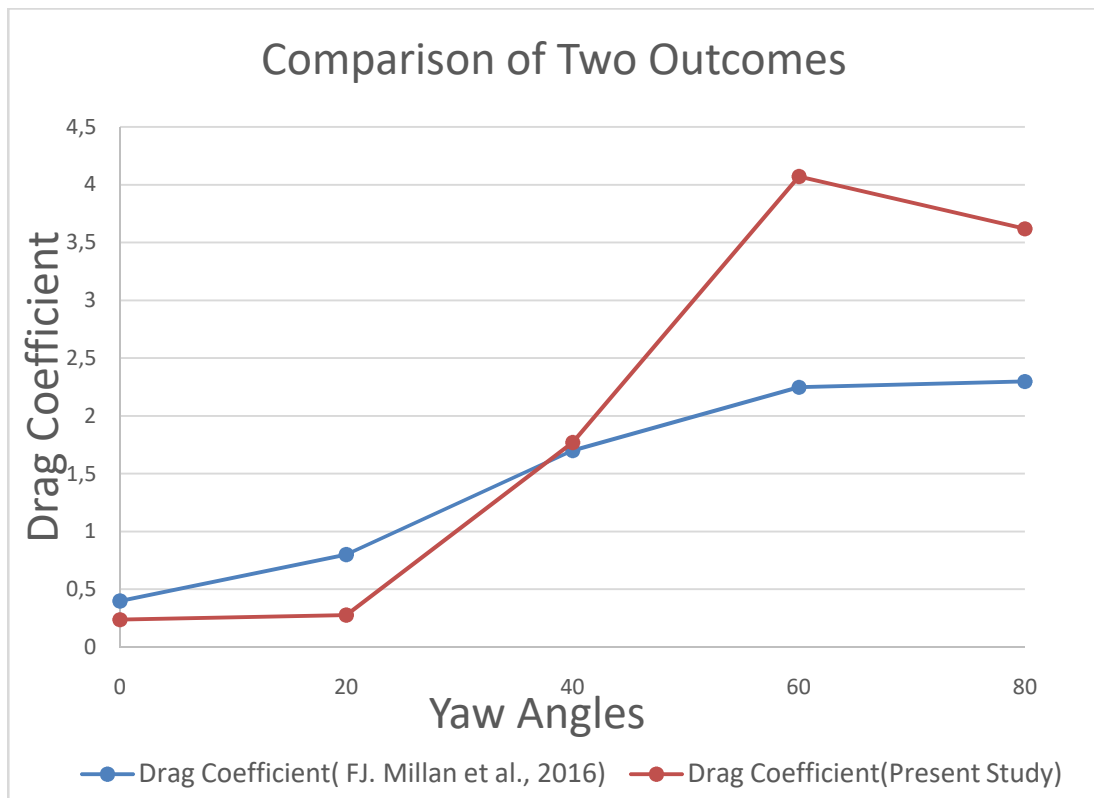


Figure 4.16: Comparison of both findings

4.3 Reynolds Number and Drag Coefficient

Now, we will draw graphs for Reynolds number and get values of drag coefficients against the particular Reynolds number. For this, first look into the below table and then we will have graphs of both the findings and then compare with one another.

For this, first Table 4.2 is shown that indicates the values of the findings. If we compare both the results, it is concluded that the CFD has given 57.35% accurate result as compared to the experimental data having different Reynolds number.

Table 4.2: Value of Drag coefficient of experimental results and the present findings against Reynolds number

Reynolds Number	C_D (F.J. Bello-Millan 2016)	C_D (Present Values)
1.68×10^5	0.43	0.65
2.3×10^5	0.42	0.65
4×10^5	0.41	0.64
6×10^5	0.38	0.63
8×10^5	0.4	0.64

Now, the graphs are shown below

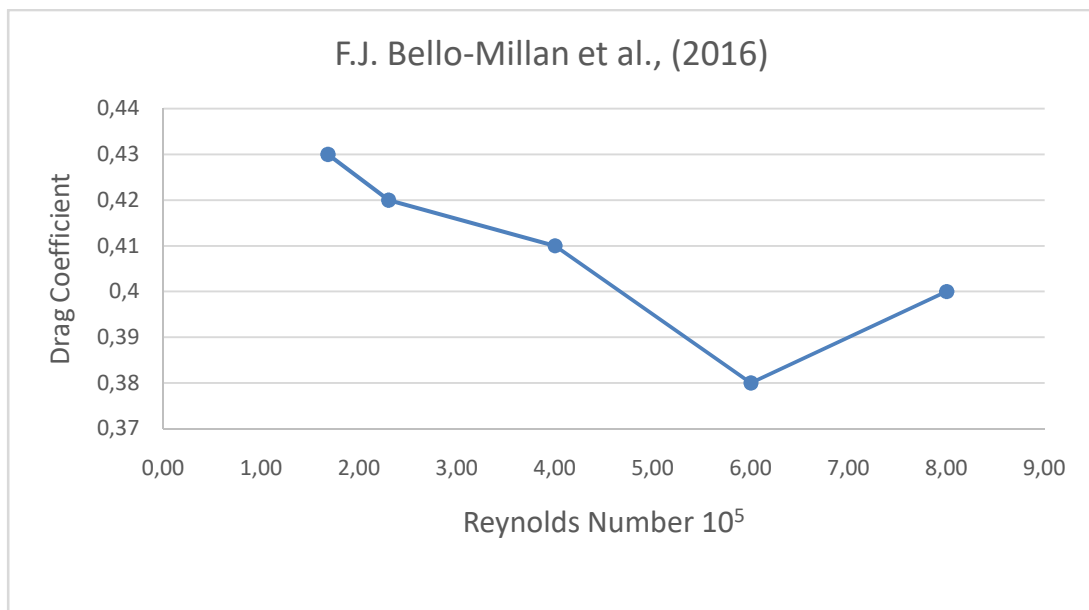


Figure 4.17: Graph of experimental result of drag coefficient and Reynolds number

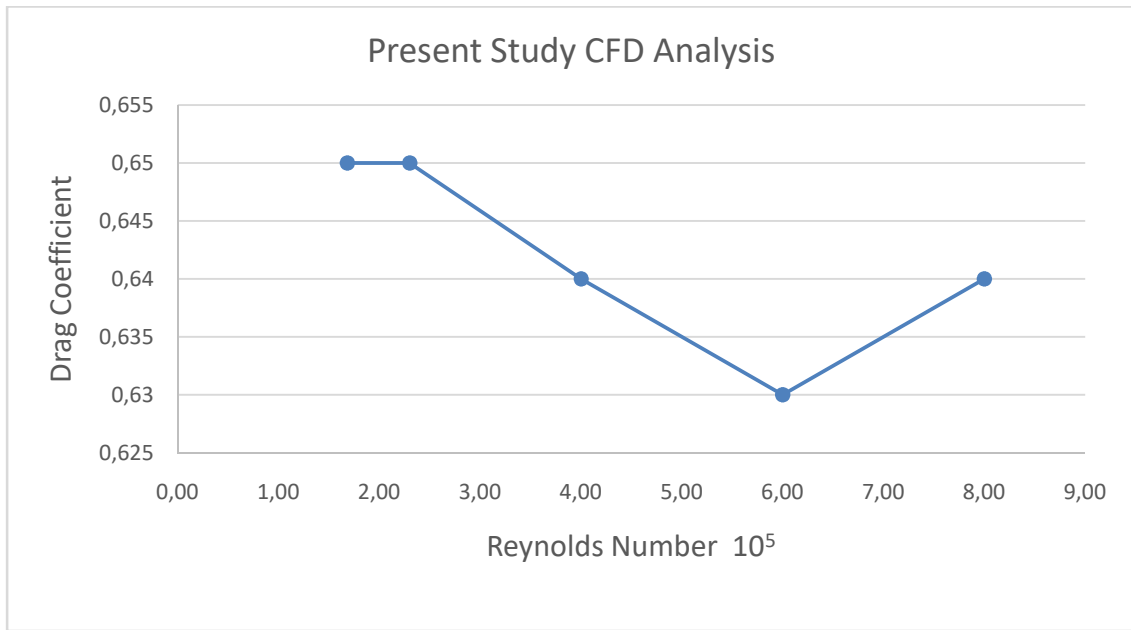


Figure 4.18: Graph of present result of drag coefficient and Reynolds number

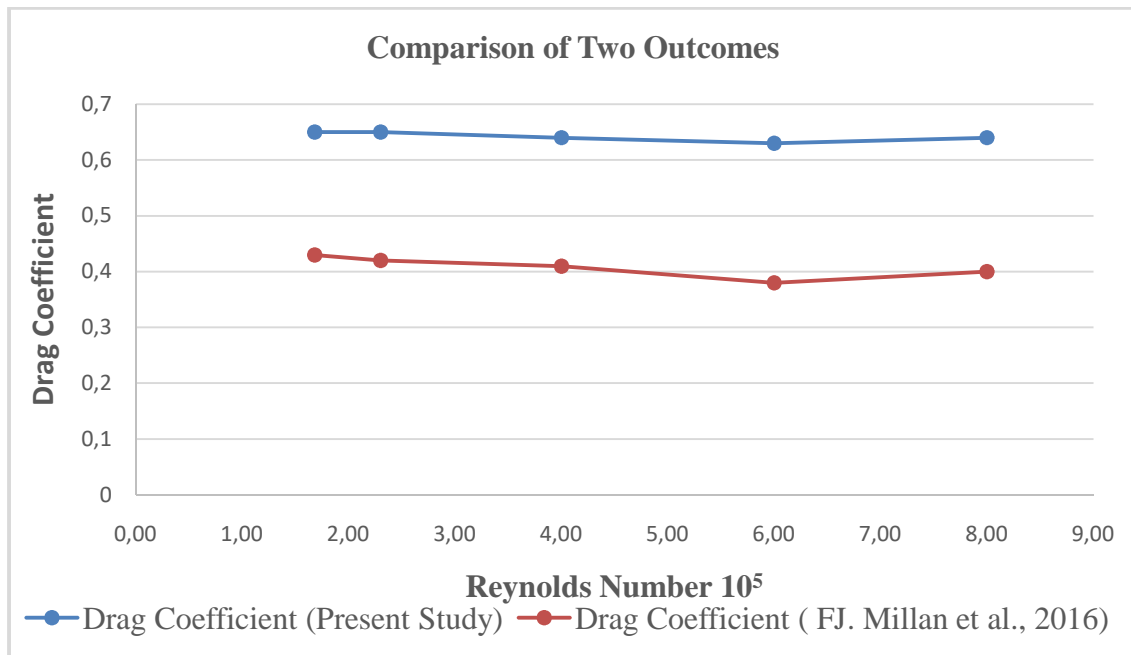


Figure 4.19: Graph of comparison of both the findings

CHAPTER 5

CONCLUSIONS AND RECOMMENDATIONS

From the above results, a conclusion was drawn. Also, recommendations are given as per the results obtained after CFD analysis is performed using FLUENT. Standard methods are followed for comparing the data obtained by CFD analysis with the experimental studies in literature.

5.1 Conclusions

It is concluded that

-) Drag coefficient declines as the Re number increases within a predefined limits of Re number.
-) In terms of yaw angles, drag coefficient increases till 60° and then starts decreasing. We have analyzed yaw angles in the range of 0° to 80° .
-) As compared to experimental results that were done previously, drag coefficient has less value than experimental results till 40° and has same value on 40° and has larger value after 40° till 80° .
-) The graphs indicates the trend of this result indicating a different direction as compared to experimental results that showed a linear relation between values of drag coefficients.
-) In order to analyze the result, velocity and pressure profiles are drawn in order to simulate drag coefficient against different yaw angles. It was observed that the flow is acceptable until 40° and after that flow is diverged in different directions which is not sufficient in order to study the Ahmed body.

5.2 Recommendations

The CFD analysis concludes an accomplishment by the author but also it raises questions. So there are following recommendations that are also necessary to make:

-) To study the drag coefficient with different range of yaw angle using CFD to see the difference in results
-) To study the effect of different Reynolds number so obtain different sets of drag coefficient and compare with the obtained results
-) Velocities other than the ones studied in this article can be analyzed

Also, different methods can be adopted to find out the drag coefficients in CFD analysis.

REFERENCES

- Ahmed, S., Ramm, G., Faltin, G. (1984). Some Salient Features of the Time-Averaged Ground Vehicle Wake. *SAE International*, 473-503
- Bayraktar, I., Landman D., Baysal, O. (2001). Experimental and Computational Investigation of Ahmed Body to Ground Vehicle Aerodynamics. *SAE Technical Paper*. 2001-01-2742. <https://doi.org/10.4271/2001-01-2742>
- Chometown, F., Strzelecki, A., L.J., Aissaoui, E. (2004). Experimental Analysis of unsteady wakes on a new simplified car model. In *5th International Colloquium on Bluff Body Aerodynamics and Applications*. Ottawa University, Canada, pp.545-548
- Chong M., Perry A., Cantwell B. (1990). A general classification of three-dimensional flow field. *Physics Fluids A2*, 765-777
- Conan B., Antoine, J., Planquart, p., (2011). Experimental aerodynamic study of a car-type bluff body. *Vol. 50, pp. 1273-1284*
- Davis, N. (2015). *FLUENT Lab Exercise 10- Ahmed Car Body*. Illinois: Computational Science and Engineering Illinois
- F.J., Bello-Millan, T., Mäkelä, L. Parras., C., delPino, C., Ferrera. (2016). Experimental study on Ahmed's body drag coefficient for different yaw angles. *J. Wind Eng. Ind. Aerodyn*157 (2016), 140-144
- Franck G., Nigro, N., Storti M., D'E;ia, J., (2009). Numerical Simulation of the flow around the Ahmed vehicle model. *Lat. Am. Apple Res.* 34(4), 295-306
- Golhke, M. Beaudoin, J. Ameilh, M. Anselmer, F. (2007). Experimental analysis of flow structures and forces on a 3D-bluff body in constant cross-wind. *Exp. Fluids* 43(4), 579-594
- Golhke, M. Beaudoin, J. Ameilh, M. Anselmer, F. (2009). Thorough analysis of vortical structures in the flow around ayawed bluff body. *J. Turbul.* 9, N15

- Guilmineau, E., Chikhaoui, O., Deng, G., Visonneau, M. (2013). Cross wind effects on a simplified car model by a DES approach. *Computers and Fluids*, vol. 78, pp. 10-23
- Han, T. (1989). Computational analysis of three-dimensional turbulent flow around a bluff body in ground proximity. *AIAA J*, 27 (9), 1213-1219
- Hinterberger, M., Gacia-Villalba, M., Rodi, W. (2004). *Large eddy simulation of flow around the Ahmed body*. Lectures Notes in Applied and Computational Mechanics- Berlin, Heidelberg
- Krajnovi , S., Davidson, L. (2005a). Flow around a simplified car, Part 1: large eddy simulation. *J. Fluid Eng.: Trans. ASME* 127 (5), 907-918
- Krajnovi , S., Bengtsson, A., Basara, B. (2011). Large eddy simulation investigation of the hysteresis effects in the flow around an oscillating ground vehicle. *J. Fluid Eng.,: Trans. ASME* 133 (12), 121103
- Krajnovi , S., Ringqvist, P., Nakade, K., Basara, B. (2012). Large eddy simulation of the flow around a simplified train moving through a crosswind flow. *J. Wind Eng, Ind. Aerodyn.* 110, 86-99
- Kuzmin, D. (2010). *A Guide to Numerical Methods for Transport Equations*. Nurenburg: Friedrich-Alexander-Universitat Erlangen-Nürnberg
- Le Good, G., Garry, K. (2004). On the Use of Reference Models in Automotive Aerodynamics. *SAE Technical Paper* 2004-01-1308
- Meile, W., Brenn, G., Reppenhagen, A., Lechner, B., Fuchs, A. (2011). Experiments and numerical simulations on the aerodynamics of the Ahmed body. *CFD Lett.* 3(1), 32-39
- Mirzaei, M., Krajnovi , S., Basara, B. (2015). Partially-averaged Navier-Stokes simulations of flows around two different Ahmed bodies. *Comput. Fluids* 117, 273-286
- Salim, S. M. & Cheah, S. C. (2009). *Wall y^+ Strategy for Dealing with Wall-Bounded Turbulent Flows*. Hong Kong, IMECS

- Serre, E., Minguéz, M., Pasquetti, R., Guilmineau, E., Bo Deng, G., Kornhaas, M., Schäfer, M., Fr lich, J., Hinterberger, C., Rodi, W. (2013). On simulating the turbulent flow around the Ahmed Body. *Comput. Fluids* 78 (20), 10-23
- Smith, R. (2008). Retrieved from http://www.engineertoolbox.com/laminar-transitional-turbulent-flow-d_577.html
- Thabet, Senan, and Thabit, Thabit H. (2018). *Computational Fluid Dynamics: Science of the Future International Journal of Research and Engineering*. Vol 5, No. 6, pp 430-433
- Volpe, R., Ferrand, V., Silva, A.D., Moyne, LL. (2014). Forces and flow structures evolution on a car body in a sudden crosswind. *J. Wind Eng. Ind. Aerodyn.* 128, 1114-125
- Wang X., Zhou, Y., Pin, Y., Chan, T. (2013). Turbulent near wake of an Ahmed vehicle model. *Exp. Fluids* 54 (4), 1490